Article

POLYMORPHS AND HYDRATES OF SEQUIFENADINE HYDROCHLORIDE: CRYSTALLOGRAPHIC EXPLANATION OF OBSERVED PHASE TRANSITIONS AND THERMODYNAMIC STABILITY

Artis Kons, Agris B#rzi#š, and Andris Acti#š

Cryst. Growth Des., **Just Accepted Manuscript** • DOI: 10.1021/acs.cgd.6b01534 • Publication Date (Web): 23 Jan 2017

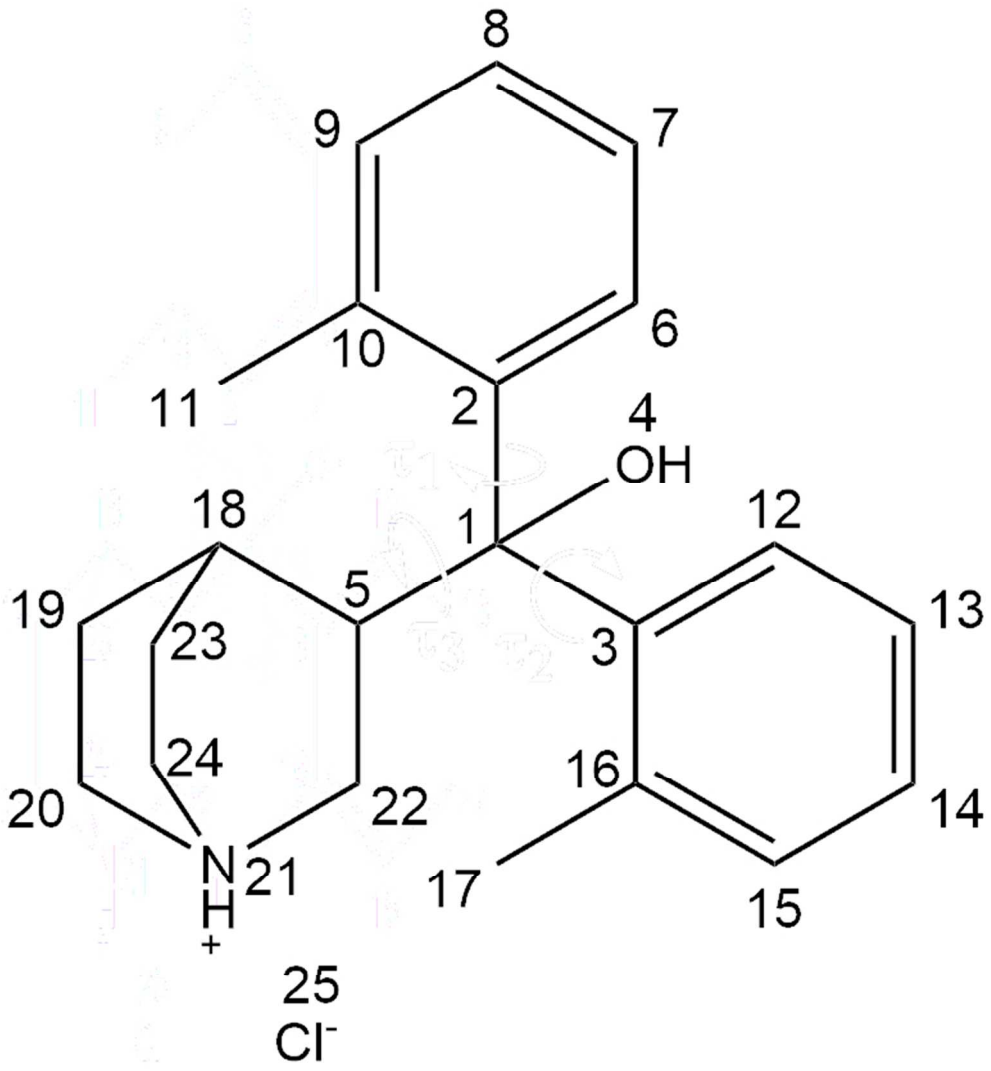

Molecular structure of sequifenadine hydrochloride with the numbering of non-hydrogen atoms and labeling of flexible dihedral angles.

66x71mm (300 x 300 DPI)

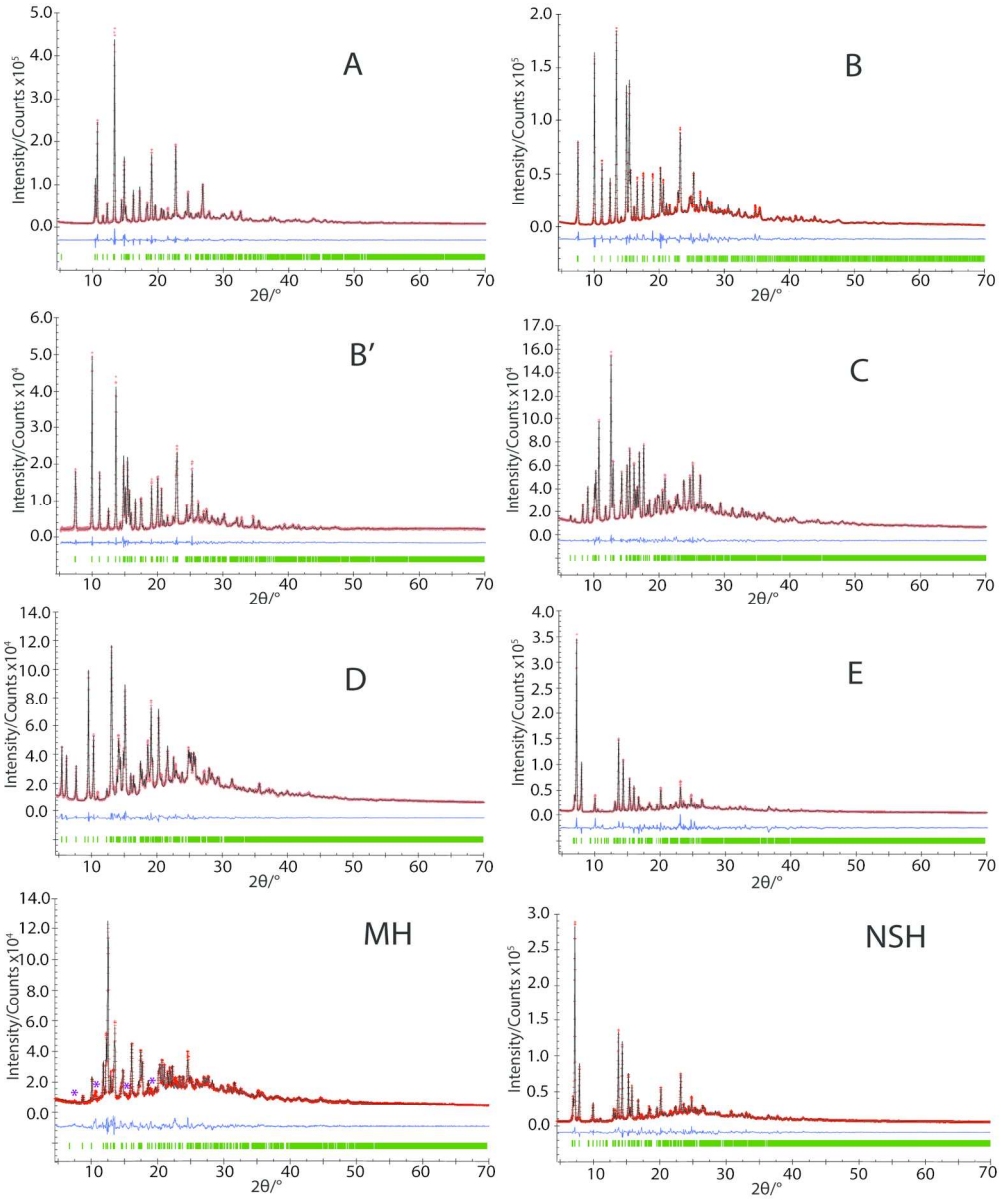

Final Rietveld fit for SQ-HCl forms A, B, B′ C, D, E, MH and NSH: red crosses - measured data points; black line - calculated profile; blue line - difference curve; green tick marks - calculated peak positions. With asterisks impurities of unknown phase in MH sample are shown.

161x195mm (300 x 300 DPI)

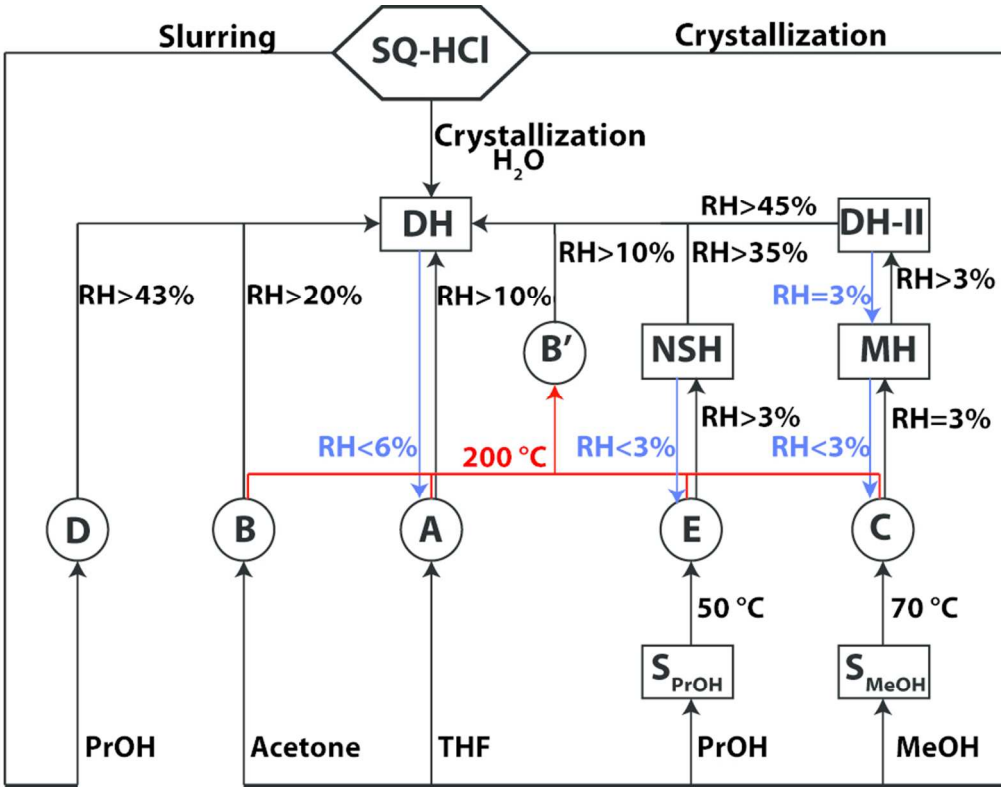

Preparation and phase transformations of SQ-HCl polymorphs and hydrates.

84x66mm (300 x 300 DPI)

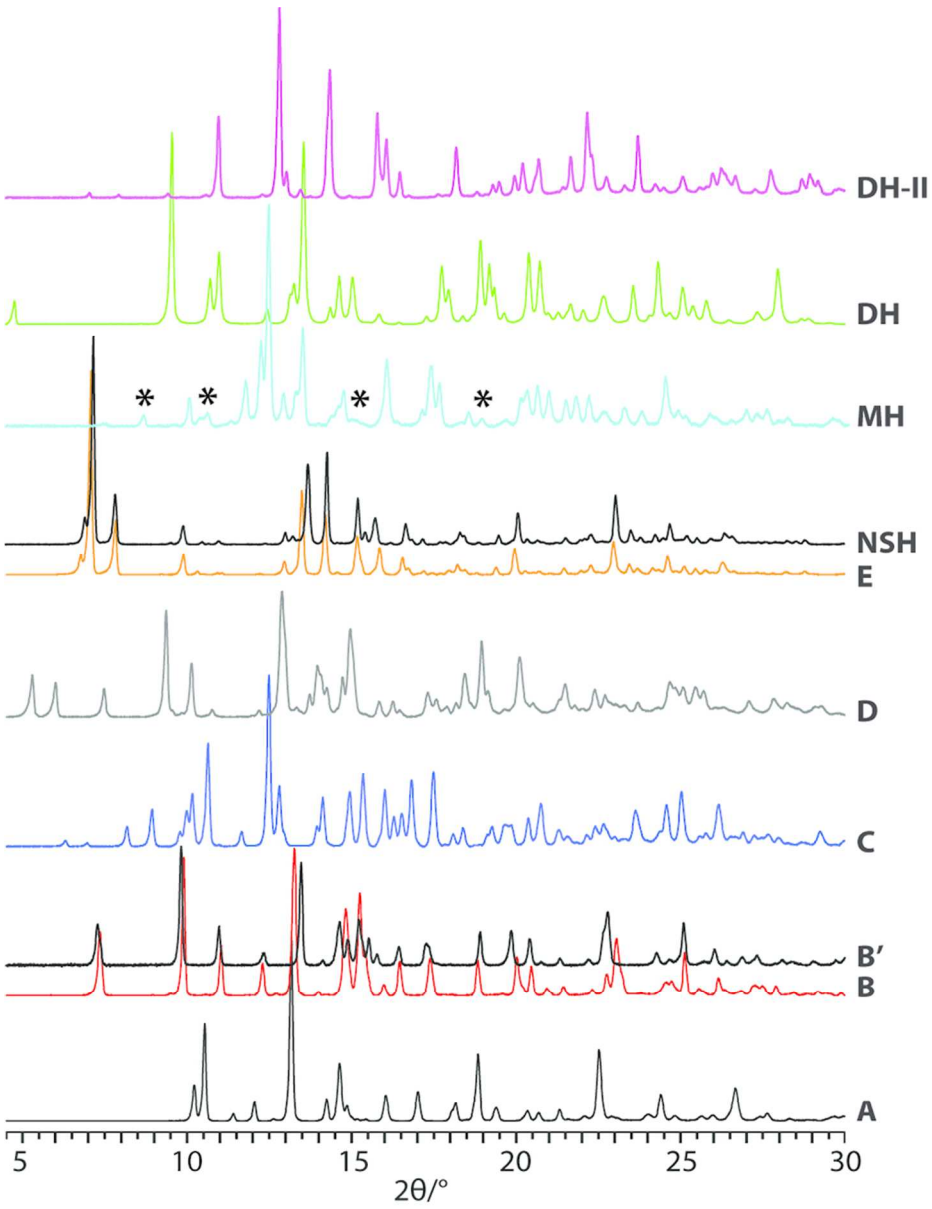

PXRD patterns of SQ-HCl crystalline forms A, B, B′, C, D, E, NSH, MH, DH, and DH-II. The signals of impurities of unknown phase are marked with black asterisks.

84x109mm (300 x 300 DPI)

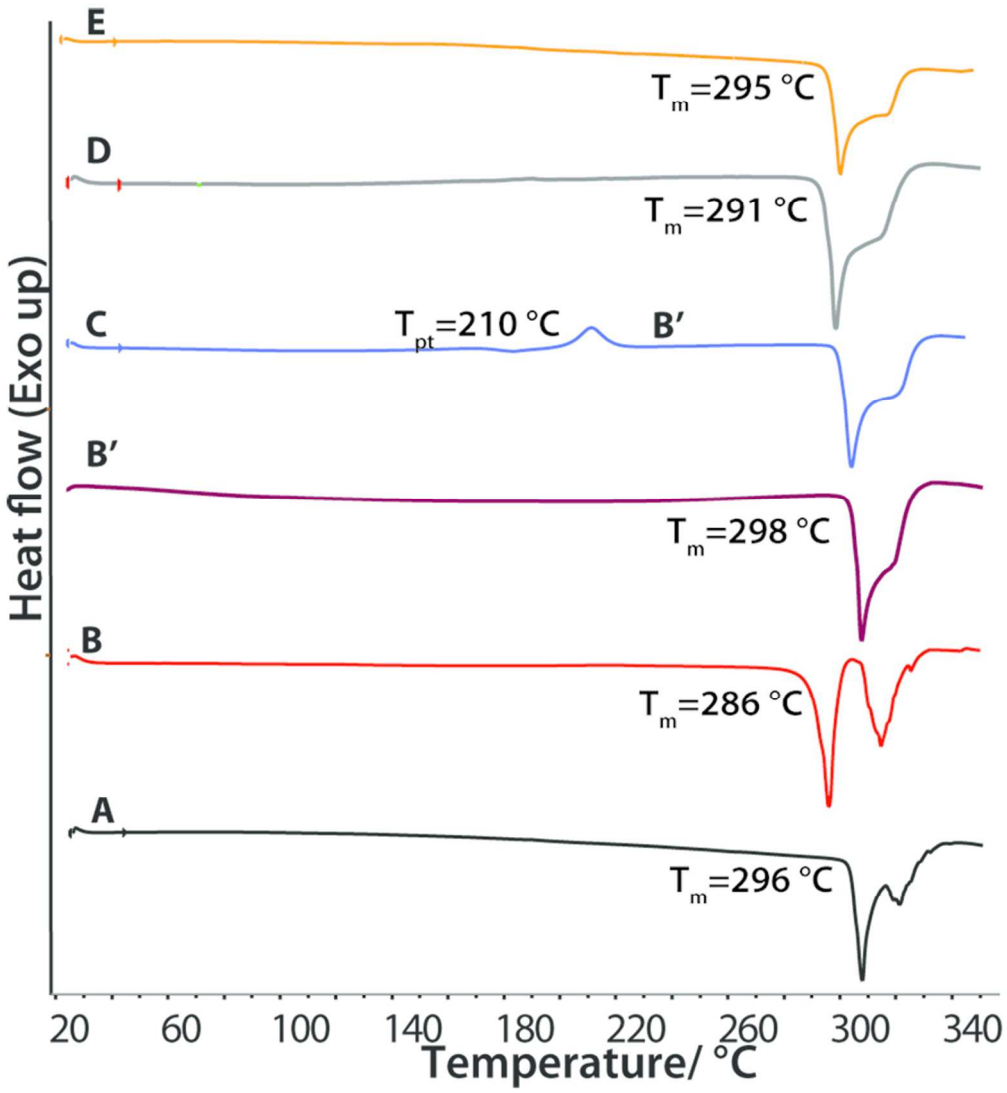

DSC curves of the SQ-HCl polymorphs (heating rate 10 °C·min-1).

84x92mm (300 x 300 DPI)

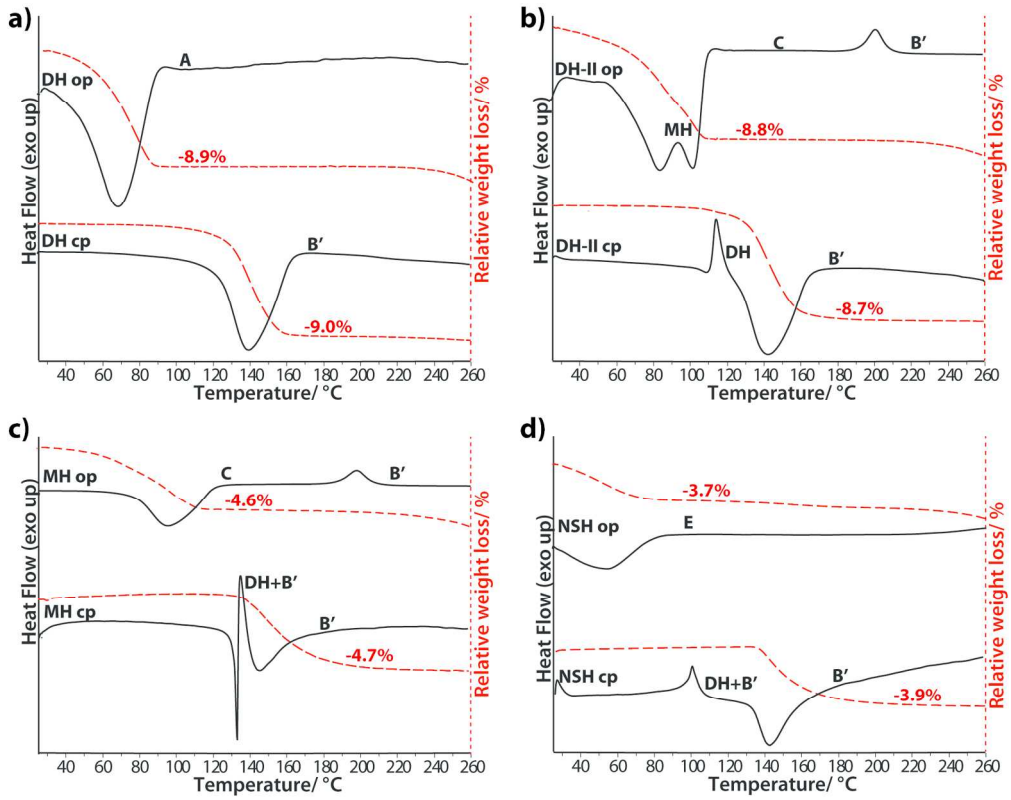

Simultaneous DSC and TGA curves (10 C·min-1) of the SQ-HCl hydrates (a) DH, (b) DH-II, (c) MH and (d) NSH in open pan (op) and closed pan (cp).

169x134mm (300 x 300 DPI)

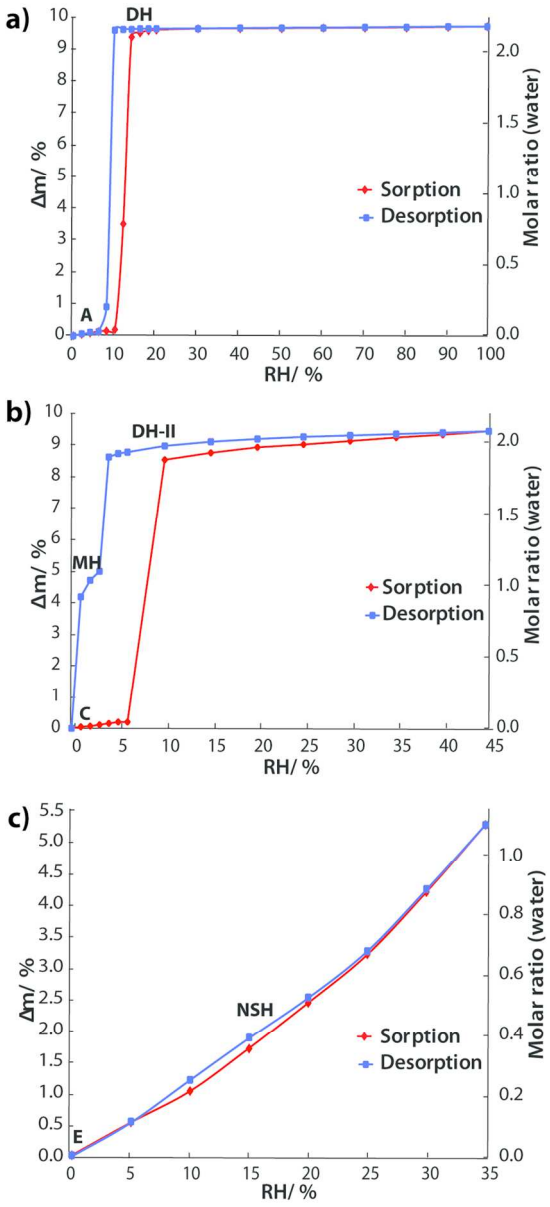

Moisture sorption and desorption isotherms of SQ-HCl forms A/DH (a), C/MH/DH-II (b) and E/NSH (c) at 25 °C.

84x187mm (300 x 300 DPI)

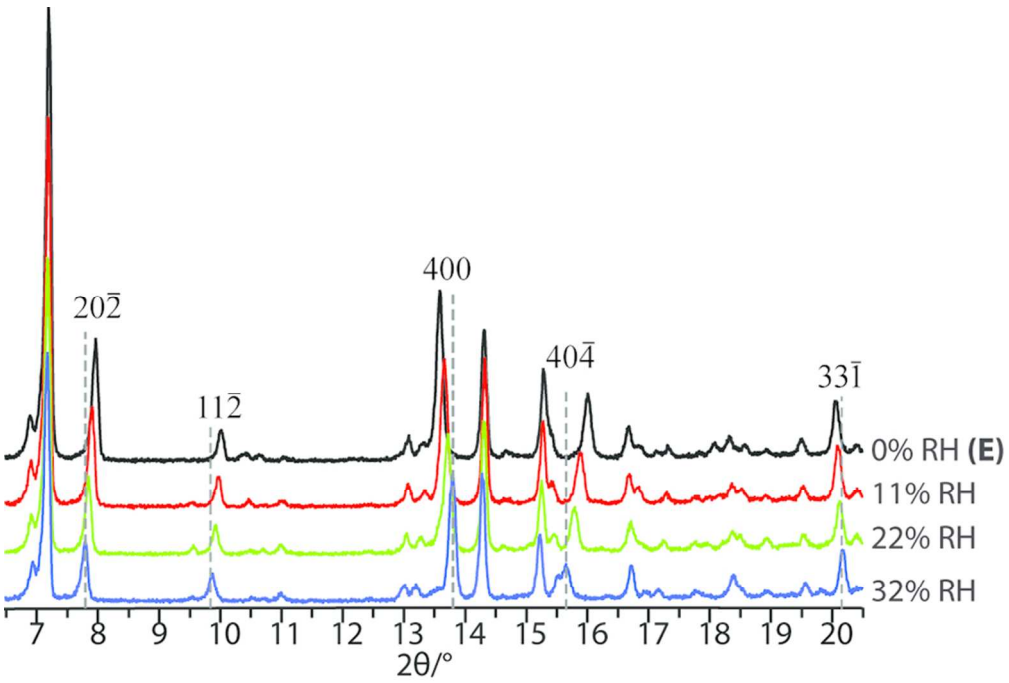

PXRD patterns of the SQ-HCl form NSH under different relative humidity conditions.

84x57mm (300 x 300 DPI)

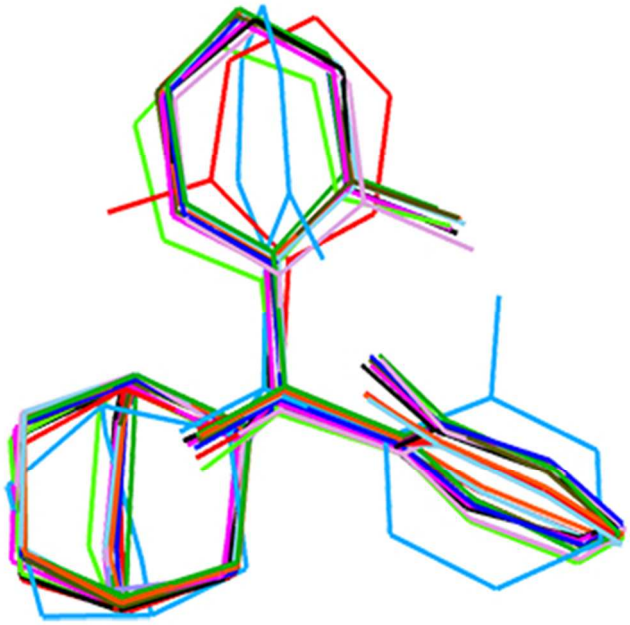

Superimposition of the sequifenadine cation geometries extracted from the crystal structures of A (black), B (green), B' (yellow), C1 (light blue), C2 (violet), D1 (blue), D2 (red), E1 (brown), E2 (orange), MH (lime) and DH (pink).

84x83mm (96 x 96 DPI)

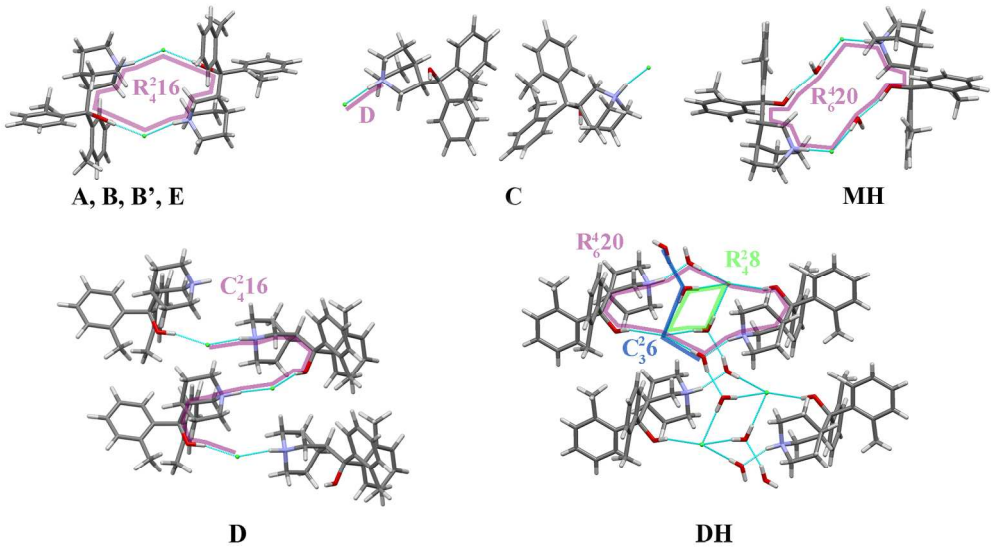

The hydrogen bonding patterns in SQ-HCl forms A, B, B', C, D, E, MH, and DH.

176x101mm (300 x 300 DPI)

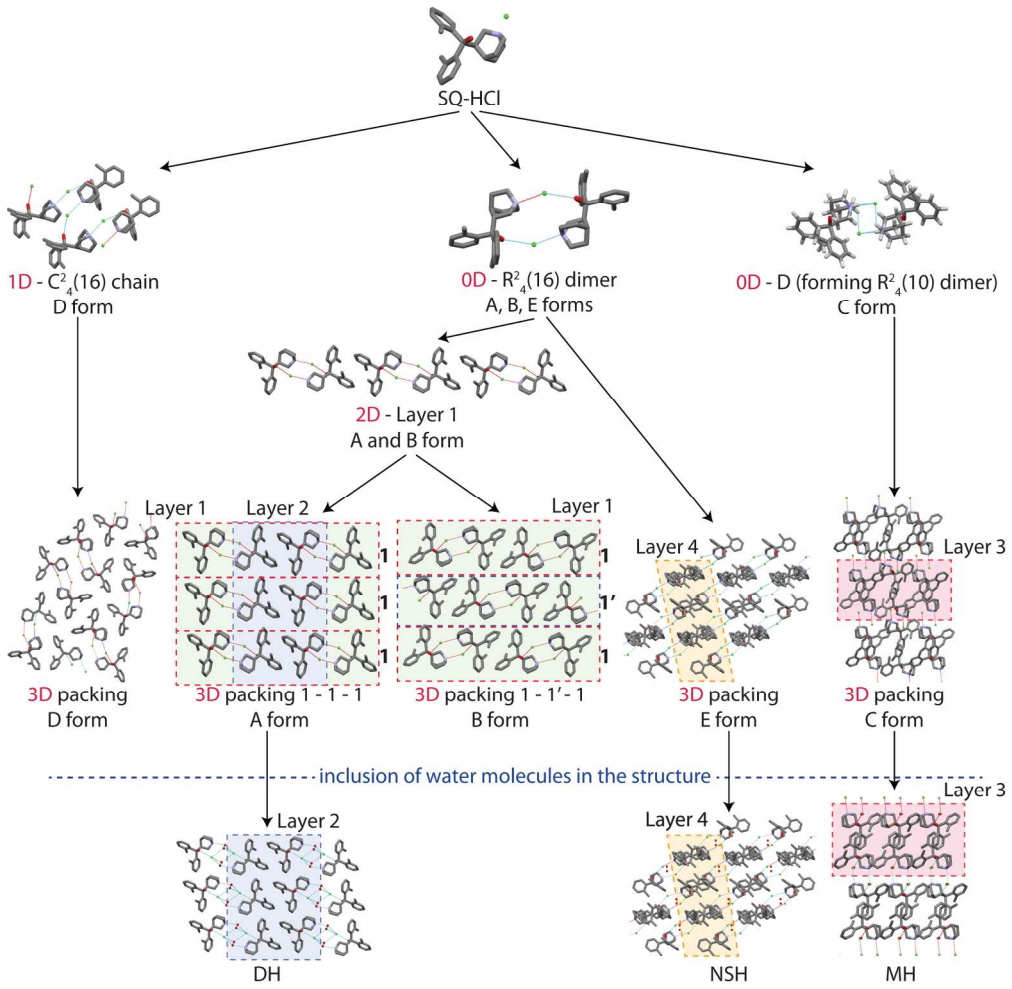

Building and packing similarities in SQ-HCl polymorphs and hydrates (layer 1 is colored green, layer 2 is colored blue, layer 3 is colored red and layer 4 is colored orange).

177x173mm (300 x 300 DPI)

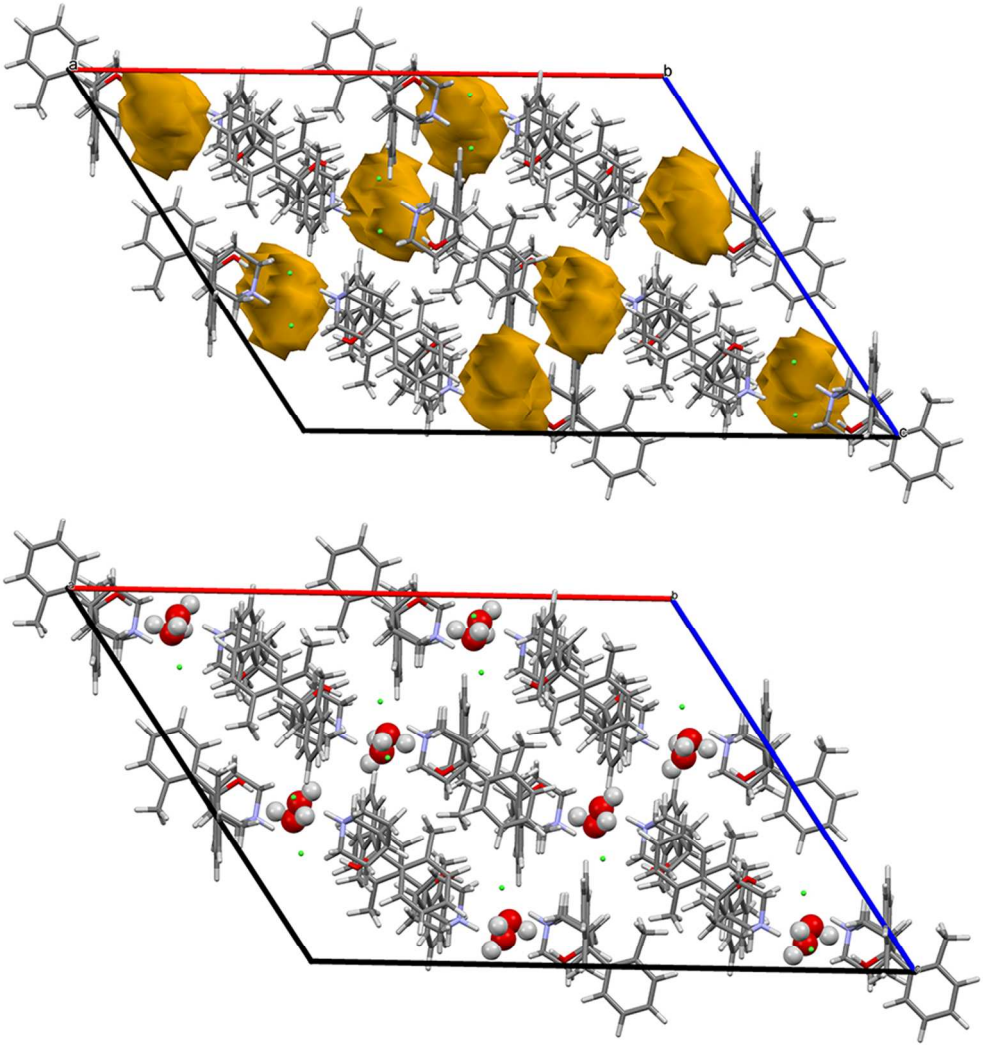

Crystal structure of form E with structure voids highlighted in brown and crystal structure of NSH with water molecules enlarged for clarity.

84x89mm (300 x 300 DPI)

POLYMORPHS AND HYDRATES OF SEQUIFENADINE HYDROCHLORIDE: CRYSTALLOGRAPHIC EXPLANATION OF OBSERVED PHASE TRANSITIONS AND THERMODYNAMIC STABILITY

Artis Kons, Agris Bērziņš and Andris Actiņš*

Faculty of Chemistry, University of Latvia, Jelgavas iela 1, Riga, LV-1004, Latvia

* Telephone: +(371)-67033907. E-mail: artis.kons@lu.lv

ABSTRACT

In this study, detailed analysis of crystal structures was used to rationalize the observed stability and phase transformations of sequifenadine hydrochloride polymorphs and hydrates, as well as to understand the observed structural diversity. The performed polymorph and hydrate screening revealed the existence of six polymorphs and four hydrates. Crystal structures of these phases were determined either from single crystal or from powder diffraction data. The different possibilities for packing of sequifenadine cations were found to be the main reason for the observed structural diversity of polymorphs. The hydrate structures were found to be structurally similar and related to those of particular polymorphs, which was consistent with the observed easy phase transitions amongst the related pairs.

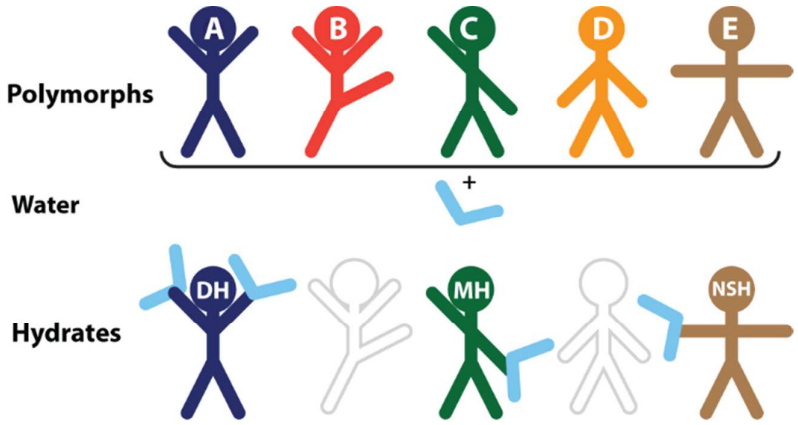

POLYMORPHS AND HYDRATES OF SEQUIFENADINE HYDROCHLORIDE: CRYSTALLOGRAPHIC EXPLANATION OF OBSERVED PHASE TRANSITIONS AND THERMODYNAMIC STABILITY

Artis Kons, Agris Bērziņš and Andris Actiņš*

Faculty of Chemistry, University of Latvia, Jelgavas iela 1, Riga, LV-1004, Latvia

* Telephone: +(371)-67033907. E-mail: artis.kons@lu.lv

ABSTRACT

In this study, detailed analysis of crystal structures was used to rationalize the observed stability and phase transformations of sequifenadine hydrochloride polymorphs and hydrates, as well as to understand the observed structural diversity. The performed polymorph and hydrate screening revealed the existence of six polymorphs and four hydrates. Crystal structures of these phases were determined either from single crystal or from powder diffraction data. The different possibilities for packing of sequifenadine cations were found to be the main reason for the observed structural diversity of polymorphs. The hydrate structures were found to be structurally similar and related to those of particular polymorphs, which was consistent with the observed easy phase transitions amongst the related pairs.

1. INTRODUCTION

Active pharmaceutical ingredients (APIs) can exist in different crystalline modifications, such as polymorphs and solvates/hydrates. Polymorphism is an ability of solids to crystallize in two or more distinct crystalline forms. Pseudopolymorphs or solvates (including hydrates) are crystalline solids that contain one or more solvent

molecules in the crystal lattice in either stoichiometric or nonstoichiometric ratio[12]. In some cases[3–5], solvates may be the only way to obtain certain polymorphs or hydrates. Screening for crystalline forms is important, because polymorphic and pseudopolymorphic transformations have been shown to affect the physicochemical properties of a compound, such as density[6], stability[7], solubility[8], and dissolution rate[9], due to the differences in crystal structures.

In general, the knowledge of polymorph and pseudopolymorph crystal structures is a prerequisite for understanding phase stability, transformations, and physicochemical properties. Although single crystal X-ray diffraction is the ultimate technique for determining the crystal structure of APIs, the main limitation of this method is the requirement of a single crystals of suitable size, quality and stability, which is not always feasible. Many crystalline solids can be obtained only as microcrystalline powders, for example, phases prepared by solid-state desolvation processes[10] and by solid state grinding[11,12]. In such circumstances, powder X-ray diffraction becomes the first choice method for structural analysis. Crystal structures can now be determined relatively easy from laboratory powder X-ray diffraction data through the development of the direct-space approach[13,14].

Sequifenadine (1-Azabicyclo[2.2.2]oct-3-yl[bis(2-methylphenyl)]-methanol) hydrochloride (Figure 1) is a H_1-receptor antagonist which also inhibits 5-HT_1 receptors of serotonin, thus decreasing the activity of allergy mediators - histamine and serotonin[15,16]. Sequifenadine is a quinuclidine derivative, which is structurally related to quifenadine [17]. To the best of our knowledge, there are no reports on the existence of polymorphs or solvates of sequifenadine hydrochloride.

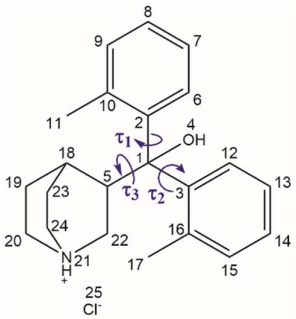

Figure 1. Molecular structure of sequifenadine hydrochloride with the numbering of non-hydrogen atoms and labeling of flexible dihedral angles.

The aims of this study were to 1) perform screening of the polymorphs and hydrates, determine their crystal structures, stability and phase transformations between them; and 2) use the obtained crystallographic information and the experimental data to rationalize the phase transformations and stability as well as packing similarities. Screening of polymorphs and hydrates was carried out using the crystallization in various solvents and by solid state transformation at different temperatures and relative humidity conditions. Stability and phase transformations amongst the obtained crystalline forms were investigated by powder X-ray diffraction, differential scanning calorimetry, thermogravimetry, variable temperature X-ray diffraction, and dynamic vapor sorption analysis. Slurry-bridging experiments at room temperature were carried out, in order to ascertain the relative thermodynamic stability of the polymorphs. Crystal structures of six polymorphs and three hydrates are presented. The phase transformations and stabilities were rationalized based on the obtained data.

2. EXPERIMENTAL SECTION

2.1. Materials

Racemic Sequifenadine hydrochloride (purity >99%) was obtained from JSC Olainfarm (Olaine, Latvia). The sample consisted of commercial dihydrate (DH) phase. Inorganic compounds and organic solvents of analytical grade were purchased from commercial sources and used without further purification.

2.2. Sample preparation

Polymorph A was obtained by recrystallization from THF or by dehydration of DH at 80 ºC/ 0 % relative humidity. Polymorph B was prepared by slow evaporation of the solution of sequifenadine hydrochloride in acetone at room temperature with relative humidity <5 %. Polymorph C was obtained by desolvation of methanol solvate at 70 ºC or by dehydration of DH-II at 80 ºC/ 0% relative humidity. Polymorph D was prepared by slurring other anhydrous forms in *n*−propanol. Polymorph E was obtained by desolvation of *n*−propanol solvate at 50 ºC. All anhydrous polymorphs were stored in desiccator with P_2O_5. Polymorph of dihydrate (DH-II) was obtained by hydration of the form C at 22 % relative humidity. Storing forms C or DH-II in desiccator with saturated CsF solution (RH=3 %) yielded monohydrate (MH), but nonstoichiometric hydrate (NSH) was obtained by hydration of the form E at 6 – 32 % relative humidity. For structure determination of NSH with monohydrate stoichiometry, the sample was loaded and sealed in capillary at RH=32%. Single crystals of DH were obtained by slow evaporation of a mixture of acetonitrile/ water (95/5 v/v) and stored at ambient conditions. Methanol solvate (S_{MeOH}) was prepared by slow cooling of hot concentrated solution of sequifenadine hydrochloride in methanol and was stored in mother liquor at ambient conditions. Slow evaporation of *n*−propanol solution at room temperature with relative humidity <5% yielded *n*−propanol solvate (S_{PrOH}).

2.3. Slurry-bridging experiments

Slurries were prepared by adding equimolar amounts (0.28 mmol) of two polymorphs (A/B; B/C etc.) to 5 mL of acetone or ethyl acetate. The slurries were shaken for 24 h at ambient temperature. Samples were withdrawn, filtered, dried over P_2O_5, and then examined by PXRD.

2.4. Powder X-ray Diffraction (PXRD)

For routine measurements the PXRD patterns were determined on a Bruker D8 Advance diffractometer using copper radiation (CuK_α = 1.54180 Å) with Bragg-Brentano geometry and LynxEye (1D) detector. The tube voltage and current were set to 40 kV and 40 mA, respectively. The divergence and anti-scattering slits were set at 0.6 mm and 8 mm, respectively. The patterns were recorded from 3° to 30° on the 2θ scale, using a scan speed of 0.2 s/0.02. To prevent the atmospheric humidity effect, samples were covered with a 10 μm polyethylene film when necessary.

VT-PXRD (variable temperature PXRD) experiments were determined on a Bruker D8 Discover diffractometer equipped with MRI temperature chamber and Asyco controller. Copper radiation (CuK_α = 1.54180 Å) with Bregg-Brentano geometry and LynxEye (1D) detector was used. The divergence and antiscattering slits were set at 0.6 mm and 8 mm, respectively. The patterns were recorded from 3° to 30° on the 2θ scale, using a scan speed of 0.5 s/0.02.

For structure determination PXRD patterns were recorded on a Bruker D8 Discover diffractometer using copper radiation (CuK_α = 1.54180 Å) in transmission mode and LynxEye (1D) detector. The tube was employed with voltage and current settings of 40 kV and 40 mA. The sample was loaded into a special glass Nr. 10 capillary (0.5 mm diameter). To Capillary spinner (60 rpm) was used to minimize instrumental and sample packing aberrations. Upper knife edge was used to reduce

the background produced by air scattering and lower knife edge was used to block the primary beam. The diffractometer incident beam path was equipped with a Göbel mirror, Soller slit, and a 0.6 mm divergence slit, while the diffracted beam path was equipped only with Soller slit. The diffraction patterns were recorded on the 2θ scale from 3 or 5 to 70° with 0.01° increments, using a scan speed of 36 s per step.

2.5. Single Crystal X-ray Diffraction (SCXRD)

The single-crystal X-ray diffraction data for sequifenadine hydrochloride DH was collected at 173 K on a Nonius Kappa CCD diffractometer using Mo Kα radiation (λ = 0.71073 Å) and Oxford Cryostream open-flow nitrogen cryostat for sample temperature control. The structures were solved by direct methods in OLEX2[18] software and refined by full-matrix least-squares on F^2 using SHELXL[19]. All non-hydrogen atoms were refined anisotropically. Mercury 3.7[20] software was used for crystal structure analysis and simulation of powder X-ray diffraction patterns, based on the crystal structure data.

2.6. Differential scanning calorimetry / thermogravimetric analysis (DSC/TGA)

DSC/TGA analyses were performed with a Mettler Toledo TGA/DSC2 instrument. Open and closed 100 μL aluminium pans were used. Heating of samples from 25 °C to 350 °C was performed at the heating rate of 10 °C·min^{-1} under a 100 mL·min^{-1} nitrogen flow. The sample mass was approximately 7-15 mg. To identify the phase that is formed after the thermal event, DSC/TG experiment was stopped just after this event and PXRD analysis of the sample was performed.

2.7. Water vapor sorption and desorption studies

Dynamic vapor sorption experiments were performed on the Surface Measurement Systems DVS Advantage. All samples (5 - 12 mg) were initially dried under a

200 mL stream of N_2 to establish the equilibrium dry mass at 25 °C. The samples were studied over a selected humidity range (from 0 - 35% RH to 0 - 100% RH) at 25 °C. Each humidity step was taken with equilibration set to dm/dt 0.002%/min on a 5 min time frame (with the minimum hold time of 10 min and the maximum of 300 min).

Additionally, water vapor sorption and desorption were studied in desiccators with controlled relative humidity (RH) by using PXRD to analyze the phase transitions taking place. To provide a variety of RH values saturated salt solutions and P_2O_5 were used. The salts used in this experiment and the corresponding RH values were CsF (3%), LiBr (6%), LiCl (11%), CH_3CO_2K (23%), $MgCl_2$ (32%), NaBr (56%), KI (68%), NaCl (75%), KCl (84%), K_2SO_4 (97%), and also P_2O_5 (~0%)[21].

2.8. Structure Determination from Powder X-ray Diffraction Data

Indexing, space group determination, structure solution and Rietveld refinement were performed using EXPO2014[22]. The unit cell dimensions were determined by applying the N-TREOR09[23] and Dicvol06[24] indexing procedures, with a set of 20-25 reflections found in 4.5°- 30° 2θ range. Space group determination was carried out using a statistical assessment of systematic absences, and Z' was determined based on density considerations. The cell and diffraction pattern profile parameters were refined according to the LeBail algorithm[25]. The background was modelled by a 20th order polynomial function of the Chebyshev type; peak profiles were described by the Pearson VII function.

The initial geometry of molecules was taken from the crystal structure of DH. The Monte Carlo / Simulating Annealing technique was used to constantly adjust the conformation, position, and orientation of the trial model in the unit cell in order to maximize the agreement between calculated and measured diffraction data.

The Rietveld refinement was carried out using soft constraints on bond distances and angles. In the Rietveld refinement, profile and cell parameters, isotropic thermal vibration, and preferred orientation parameters (using March-Dollase model[26,27]) were optimized to get the optimal crystal structure. The planar phenyl ring was treated as a rigid body and soft constraints on bond distances and angles were used. The final Rietveld refinement showed a good agreement between the observed and the calculated profiles (Figure 2). Relevant crystal data and refinement details for A, B, B', C, D, E, NSH, MH and DH are summarized in Table 1.

Table 1. Crystal data for SQ-HCl forms

	A	**B**	**B'**	**C**	**D**	**E**	**NSH** (at RH=32%)	**MH**	**DH**	**DH-II**
Empirical formula	$C_{22}H_{28}NOCl$	$C_{22}H_{28}NOCl$	$C_{22}H_{28}NOCl$	$C_{22}H_{28}NOCl$	$C_{22}H_{28}NOCl$	$C_{22}H_{28}NOCl$	$C_{22}H_{30}NO_2Cl$	$C_{22}H_{30}NO_2Cl$	$C_{22}H_{32}NO_3Cl$	$C_{22}H_{32}NO_3Cl$
Formula weight	357.90	357.90	357.90	357.90	357.90	357.90	375.92	375.92	377.81	377.81
Sample type	Powder	Powder	Powder	Powder	Powder	Powder	Powder	Powder	Single crystal	Powder
Crystal system	Triclinic	Triclinic	Triclinic	Monoclinic	Monoclinic	Monoclinic	Monoclinic	Monoclinic	Triclinic	Monoclinic
Space group	*P–1*	*P–1*	*P–1*	*P21/c*	*P21/n*	*C2/c*	*C2/c*	*C2/c*	*P–1*	*C2/c*
a, Å	*7.0130(4)*	*7.2303(16)*	*7.1647(11)*	*13.7397(6)*	*7.0114(16)*	*31.182(5)*	*31.017(4)*	*28.689(17)*	*6.8261(2)*	*25.8323(8)*
b, Å	*8.5448(5*	*11.820(2)*	*11.949(2)*	*11.7290(5)*	*28.655(6)*	*14.653(2)*	*14.612(2)*	*11.009(5)*	*8.5259(2)*	*12.1918(4)*
c, Å	*17.3156(10)*	*12.041(4)*	*11.9707(17)*	*24.9421(11)*	*19.732(5)*	*22.617(4)*	*22.933(4)*	*14.505(7)*	*18.7897(5)*	*14.1149(50*
α, °	*91.524(3)*	*95.644(12)*	*95.976(9)*	*90*	*90*	*90*	*90*	*90*	*98.3460(10)*	*90*
β, °	*99.332(3)*	*99.357(10)*	*91.450(8)*	*96.229(3)*	*95.933(17)*	*123.624(8)*	*123.988(6)*	*114.33(3)*	*94.7400(10)*	*108.196(5)*
γ, °	*103.955(2)*	*92.580(12)*	*97.993(9)*	*90*	*90*	*90*	*90*	*90*	*101.9530(15)*	*90*
V, $Å^3$	*991.34(10)*	*1008.5(4)*	*1008.5(3)*	*3995.8(3)*	*3943.2(16)*	*8605(3)*	*8618(2)*	*4174(4)*	*1051.30(5)*	*4223.1(13)*
ρ_{calc}, $g \cdot cm^{-3}$	1.199	1.179	1.179	1.190	1.206	1.105	1.159	1.196	1.245	1.239
Z/ Z'	*2/1*	*2/1*	*2/1*	*8/2*	*8/2*	*16/2*	*16/2*	*8/1*	*2/1*	*8/1*
Temperature, K	293(2)	293(2)	293(2)	293(2)	293(2)	293(2)	293(2)	293(2)	173(2)	293(2)

$2\theta_{min}$–$2\theta_{max}$ /increment, °	4.5–70.0/ 0.01	4.5–70/ 0.01	5.0–70/ 0.01	4.5–70/0.01	4.5–70/0.01	4.5–70/0.01	4.5–70/ 0.01	4.5–70/0.01	-	4.5–70/ 0.01
Rwp	0.0501	0.0606	0.0387	0.0277	0.0547	0.0685	0.0551	0.0609	-	-
Rp	0.0354	0.0416	0.0260	0.0203	0.0382	0.0494	0.0386	0.0418		-
R_{exp}	0.0074	0.0083	0.0108	0.0079	0.0081	0.0095	0.0091	0.0093		
R_1 (wR_2), %	-	-	-	-	-	-	-	-	5.18 (11.93)	-
Total cell energy, $kJ \cdot mol^{-1}$ (relat. to form D)	7.9	8.0	10.2	20.0	0	8.3	-	-	-	-

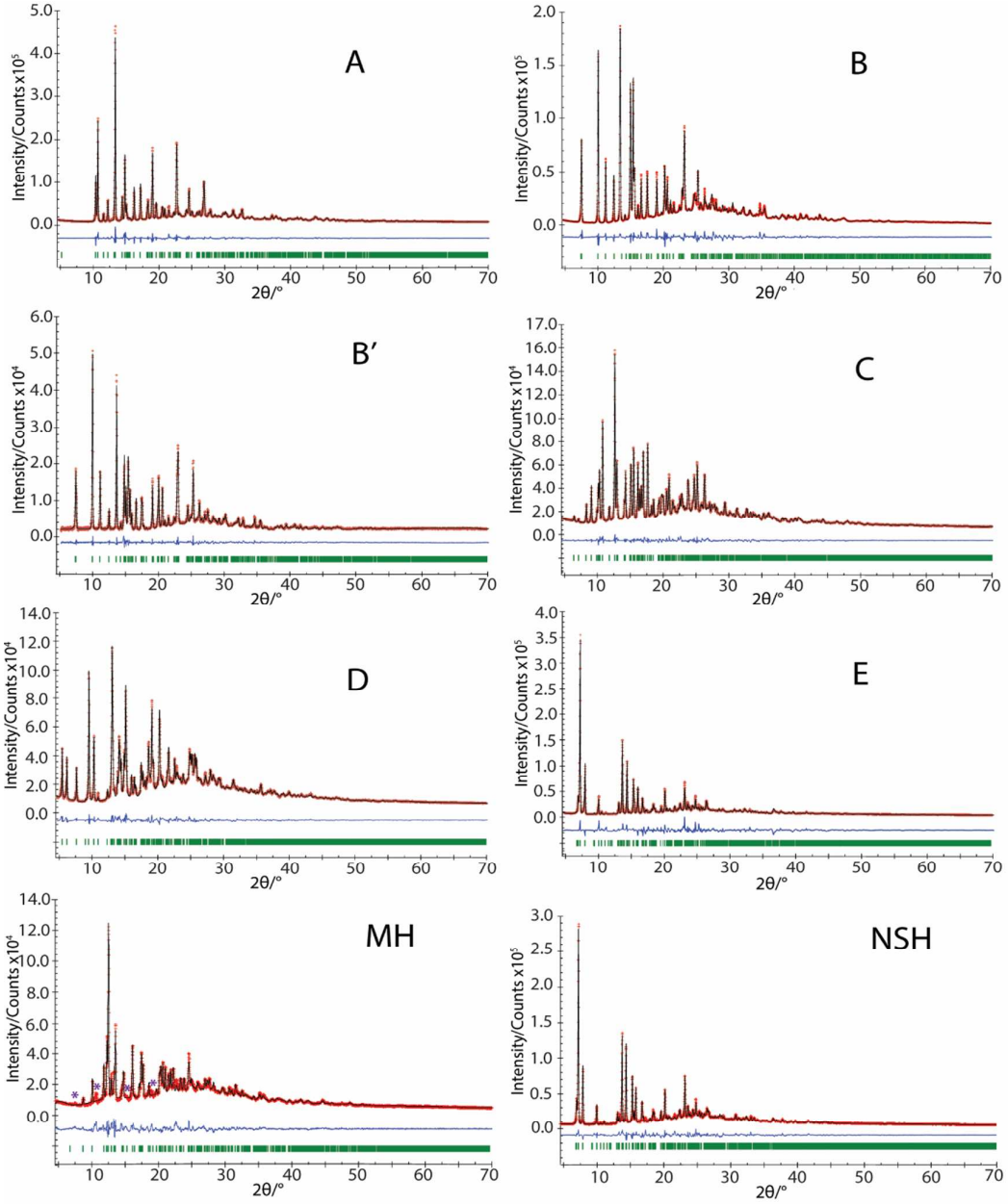

Figure 2. Final Rietveld fit for SQ-HCl forms A, B, B' C, D, E, MH and NSH: red crosses - measured data points; black line - calculated profile; blue line - difference curve; green tick marks - calculated peak positions. With asterisks impurities of unknown phase in MH sample are shown.

2.9. Theoretical Calculations.

Geometries of the A, B, B', C, D and E crystal structures were optimized using the DFT PWscf package within Quantum ESPRESSO[28]. Calculations were performed with the PBE[29] exchange correlation functional with vdW interactions treated according to the D2 method of Grimme[30], and ultra-soft pseudopotentials with a wave function cut-off of 44 Ry. Pseudopotential files C.pberrkjus.UPF, H.pbe-rrkjus.UPF, N.pbe-rrkjus.UPF, O.pberrkjus.UPF and Cl.pbe-n-van.UDF were acquired from the Quantum ESPRESSO pseudopotential data base[31]. Pseudopotentials, energy and force thresholds for structural relaxation were used as described in literature[32]. A k-point grid of 2 x 2 x 2 was used.

Conformer and pairwise interaction energies were calculated in Gaussian09[33] using B3LYP /6-311G (d,p) level set to molecular geometries directly extracted from the crystal structures after the geometry optimization in Quantum ESPRESSO. The basis set superposition error was corrected using the counterpoise method. The interaction energy was calculated as the difference between the total energy of the dimer and the corresponding isolated moieties.

3. RESULTS AND DISCUSSION

3.1. Screening. The crystal form screening experiments reveal the existence of at least six SQ-HCl polymorphs (**A, B, B', C, D, E**), two dihydrates (**DH** and **DH-II**), a monohydrate (**MH**), a nonstoichiometric hydrate **(NSH**) and also numerous solvated forms which will be reported in a following paper. The polymorphs and the dihydrates were designated according to their chronological order of discovery. Figure 3 shows a flowchart illustrating the different polymorphs and hydrates discovered, their preparation and observed phase transitions (*n*-propanol and ethanol solvates S_{PrOH} and S_{MeOH} are also included, since polymorphs E and C are obtained by their desolvation).

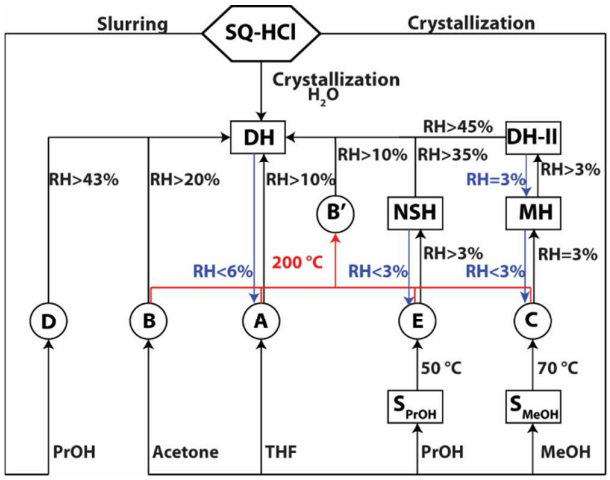

Figure 3. Preparation and phase transformations of SQ-HCl polymorphs and hydrates.

It can be seen that polymorphs A and B are crystallized from different solvents, polymorph D is obtained by slurring anhydrous SQ-HCl in *n*-propanol, two other polymorphs E and C are obtained by desolvation of particular SQ-HCl solvates, whereas polymorph B' is obtained by exposing other SQ-HCl polymorphs (except for the D) to an elevated temperature. All of the hydrates are obtained by exposing particular SQ-HCl polymorphs or lower stoichiometry hydrates to a specific relative humidity.

Overlay of the PXRD patterns of SQ-HCl crystalline forms is depicted in Figure 4. Each form has a unique and distinguishable PXRD pattern, except for pairs B/B' and E/NSH, where the PXRD patterns are distinguishable only by small peak shifts to lower or higher 2θ values. Note that highly similar PXRD patterns suggested very high structural similarity between forms B/B' and also between forms E/NSH. The sample of MH contains an impurity from an unknown phase (marked by black asterisks in Figure 4).

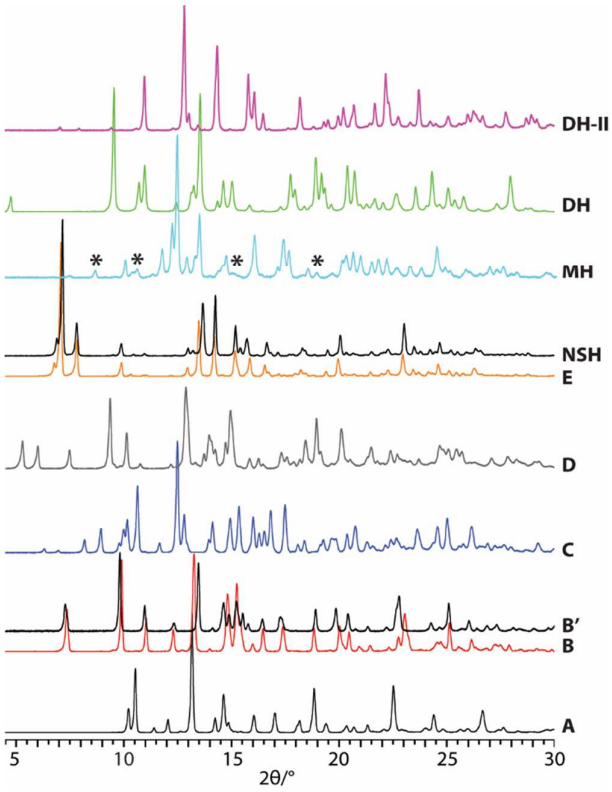

Figure 4. PXRD patterns of SQ-HCl crystalline forms A, B, B', C, D, E, NSH, MH, DH, and DH-II. The signals of impurities of unknown phase are marked with black asterisks.

3.2. Thermal Characterization. Figure 5 shows the DSC curves for the polymorphs of SQ-HCl. All polymorphs (except B and C) display two overlapping endothermic effects associated with the melting process, immediately followed by decomposition. These results indicate, that the melting temperatures (determined from the onset of the respective peaks) of polymorphs A, B, B', D and E range from 286 °C to 298 °C. Interestingly, structurally closest polymorphs B and B' (see section 3.5) have the most diverse melting temperatures. For the form C, an exothermic peak at 210 °C is observed prior to the melting / decomposition peaks. This exothermic peak corresponds to a phase transition from C to B', as confirmed by PXRD analysis,

which substantiates the monotropic relationship between these polymorphs on the basis of the heat of transition rule [34]. However, it was not possible to determine the thermodynamic relationships for other polymorphic pairs due to the coinciding melting and decomposition processes (making it impossible to directly measure the enthalpy of fusion).

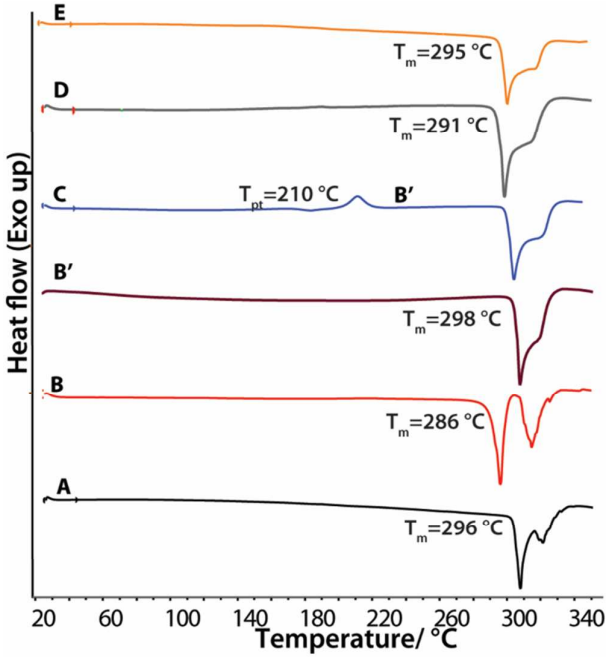

Figure 5. DSC curves of the SQ-HCl polymorphs (heating rate 10 °C·min^{-1}).

Simultaneous DSC/ TGA analyses of forms DH, DH-II, MH, and NSH were performed by using both open and closed pans, for more comprehensive characterization of the transformations taking place during the dehydration. Observed weight loss confirmed the given stoichiometry and are given in Table 2 together with the dehydration products.

A single dehydration endotherm of form DH was observed under both conditions with a peak temperature of 70 °C in the open pan and 140 °C in the closed pan (Figure 6a). Observed weight loss confirmed the dihydrate stoichiometry. The

dehydration product in the open pan was polymorph A, while in the closed pan it was form B', as confirmed by the PXRD analysis.

Table 2. Observed and calculated weight loss, and dehydration products of SQ-HCl hydrates

Hydrate	Stoichiometry	Observed, %	Calculated, %	Dehydration product
DH	1:2	8.9-9.0	9.1	A
DH-II	1:2	8.7-8.8	9.1	C
MH	1:1	4.6	4.8	C
NSH	1:1	3.7-3.9[a]	4.8	E

[a] – when stored in ~25% RH at 25°C.

When form DH-II was dehydrated using the open pan (Figure 6b), two-step dehydration was observed as two overlapping endothermic peaks, with peak temperatures of 79 °C and 96 °C. Despite the absence of distinct steps in TGA plot, the presence of two endothermic peaks is due to the formation of an intermediate monohydrate MH, with the final dehydration product being the polymorph C, as confirmed by the PXRD analysis. Following exothermic event with a peak temperature of 200 °C is already observed phase transition from the form C to B'. When heating was performed using closed pan, a different thermal plot was obtained. Before the dehydration an exothermic effect at 107 °C was observed. This exothermic peak is attributed to a solid-state phase transition from form DH-II to DH, as confirmed by the PXRD analysis. This observation substantiates that DH is thermodynamically more stable than DH-II. Following endothermic peak at 140 °C (peak temperature) is attributed to the dehydration of DH. The dehydration product under these conditions is also the form B'. Therefore, in closed pans dehydration of DH always produced B'.

Simultaneous DSC/ TGA curves of MH are shown in Figure 6c. In open pan dehydration of MH was observed as single broad endothermic peak in the DSC with peak temperature of 97 °C and associated weight loss of 4.6% in the TGA. However, in closed pan a sharp endothermic signal immediately followed by an exothermic signal was observed just before the dehydration. We suggest that the sharp endothermic effect with peak temperature of 123 °C is attributed to congruent melting or decomposition and the following exothermic effect with peak temperature of 128 °C is associated with crystallization of a mixture of forms DH and B' as confirmed by the PXRD analysis. The final endothermic peak at 138 °C is attributed to the dehydration of DH by producing polymorph B' as the dehydration product.

Simultaneous DSC/ TGA curves of NSH are shown in Figure 6d. In open pan a single broad dehydration endotherm between room temperature and 80 °C was observed. Within this interval, the associated weight loss for NSH with maximum water content was 3.7%. However, in closed pan NSH showed an exothermic peak at around 100 °C and broader endothermic peak at around 140°C. The exothermic peak is attributed to the decomposition of NSH to a mixture of forms DH and B', as confirmed by the PXRD analysis. The endothermic peak, associated with weight loss of 3.9%, was due to the dehydration of DH to B'.

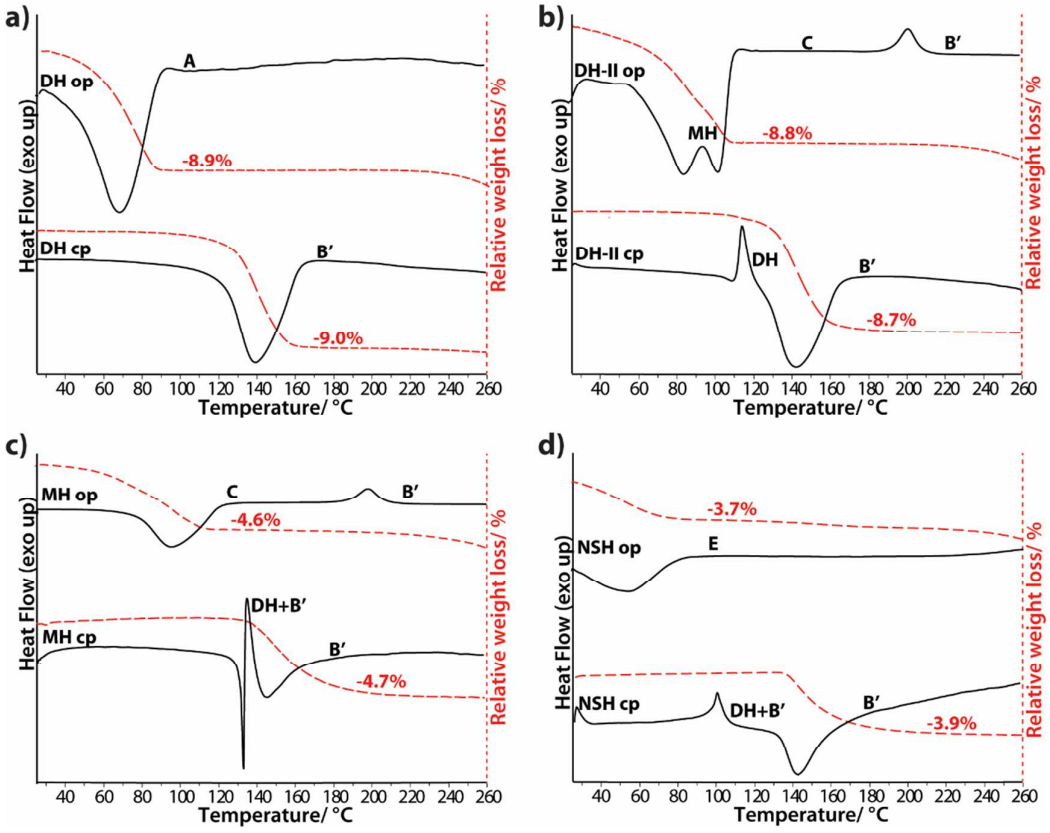

Figure 6. Simultaneous DSC and TGA curves (10 C·min^{-1}) of the SQ-HCl hydrates (a) DH, (b) DH-II, (c) MH and (d) NSH in open pan (op) and closed pan (cp).

3.3. Thermodynamic stability of SQ-HCl polymorphs. The thermodynamic stability order of polymorphs was established by comparing computed total cell energies, using periodic DFT calculations in Quantum ESPRESSO and phase transitions occuring in slurry-bridging experiments. Total cell energies (Table 1) of forms A, B, B', C, D and E indicate, that the form D is the most stable form, whereas the form C is the least stable form, having the highest total cell energy of 20.0 kJ·mol^{-1} (relative to form D). Total cell energies of forms A, B, B' and E (7.9, 10.2 8.0, and 8.3 kJ·mol^{-1}, respectively) are too close to infer the stability relationships. Slurry-

bridging experiments were carried out at ambient temperature. Due to the solvate formation with numerous different solvents, mixtures of polymorphs were slurred only in acetone and ethyl acetate to avoid the solvate formation. A summary of the results from the slurry-bridging experiments is given in Table 3. These observations demonstrate that the form D is the most thermodynamically stable form at ambient temperature, followed by forms B and A having progressively lower stability. However, that relative stability between the forms B', C and E is unclear, but by combination of results from experimental and computational studies it is reasonable to conclude that thermodynamic stability at ambient temperature follows the order of D >B>A>E>C.

Additionally, a comparison of the thermal stability of forms A, B, C D and E at an elevated temperature was performed by VT-PXRD (see S1-S5, Supporting Information). VT-PXRD patterns show that upon heating all polymorphs, except for the D, transformed to B'. The polymorph A is relatively stable between 30 – 220 °C, however, as the sample was heated at 220 °C for 2 h, characteristic peak of polymorph B' appeared and complete transformation to B' was observed in 16 h. PXRD profile of the form C was relatively unchanged between 30 – 140 °C, after which the sample transformed to B' at 150 °C. The polymorph E was relatively stable between 30 – 100 °C, after which sample gradually transformed into B', with complete transformation occurring at 190 °C.

Table 3. Results of the slurry-bridging experiments

Mixture	Resulting phase
A/D	D
B/D	D

B'/D	D
C/D	D
D/E	D
A/B	B
A/B'	B
B/B'	B
B/C	B
B/E	B
B'/C	B
B'/E	B
C/E	B
A/C	A
A/E	A

3.4. Dynamic Vapour Sorption (DVS) experiments. The hydration and dehydration behavior of A/DH, C/MH/DH-II and E/NSH was investigated by moisture sorption/desorption experiments by determining both the weight change (using DVS) and the phase composition (using PXRD) of the samples.

As shown in Figure 7a, form A undergoes full hydration to DH at 14% RH with weight gain of 9.4 %, consistent with the formation of dihydrate. No significant mass change was observed with further increase of RH. The dehydration of DH occurs only at RH = 8%, indicating the high stability of DH. The single step hydration and dehydration, as well as the stoichiometric number of incorporated water molecules are characteristic of stoichiometric hydrates. Small hysteresis (~6% RH) between the sorption and desorption isotherms shows that there is almost no kinetically controlled

delay between the hydration and dehydration and this reversible phase transition has low energy barrier, suggesting that crystal structures of these two forms are likely to be similar.

The moisture sorption/desorption isotherms of forms C/MH/DH-II (Figure 7b) show one step stoichiometric hydration and two step dehydration. Anhydrous form C is stable in 0 - 6% RH range. When RH is increased to 10%, mass increases by 8.5%, consistent with the formation of dihydrate. Small mass increase up to 9.3% from the initial mass was observed with further increase of RH. Form DH-II is stable only up to 45 % RH, and at higher RH it irreversibly transforms to DH. The first dehydration step of DH-II occurs at RH = 3% and lower hydrate is obtained in these conditions. The observed weight change of 4.1 – 4.9% is consistent with monohydrate stoichiometry and using PXRD analysis the dehydration product was confirmed to be MH. MH is stable only in narrow RH range (3 – 1%). When RH was decreased to 0% further dehydration process was observed and anhydrous form C was obtained. Similar to A/DH system, there is only small kinetically controlled delay between hydration and dehydration as observed by the small hysteresis (~7% RH) between the sorption and desorption isotherms.

Figure 7c shows sorption/desorption isotherms for forms E/NSH. During the sorption/desorption experiment the mass gradually changed depending on the RH, indicating that NSH is a nonstoichiometric hydrate. The maximum weight gain of 5.4 % was observed in 35% RH, which corresponds to ~1.2 mol of water per mol of SQ-HCl. Under higher RH, NSH irreversibly transforms to DH. PXRD analysis of sample in variable humidity were performed to confirm that form NSH is a nonstoichiometric hydrate, and that the continuous change of mass in the sorption/desorption experiments is not caused by the adsorption of water in the sample. The results

showed that peak positions and intensities changed by changing the relative humidity (Figure. 8). Such variation of PXRD pattern is characteristic for nonstoichiometric hydrates, where water molecules can absorb and desorb form crystal structure without introducing any significant changes, and confirms that form E is its isostructural dehydrate.

Moisture sorption analysis of forms B and D showed that these forms were stable up to 22% and 43% RH, respectively. Under higher RH irreversible transformation to form DH was observed.

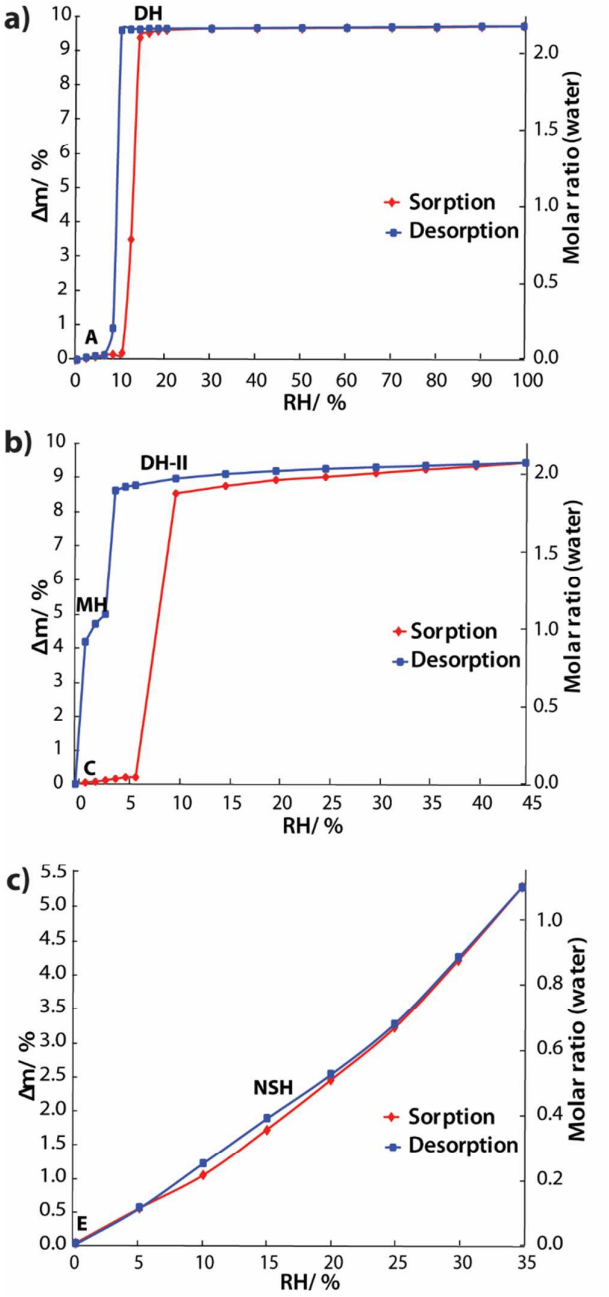

Figure 7. Moisture sorption and desorption isotherms of SQ-HCl forms A/DH (a), C/MH/DH-II (b) and E/NSH (c) at 25 °C.

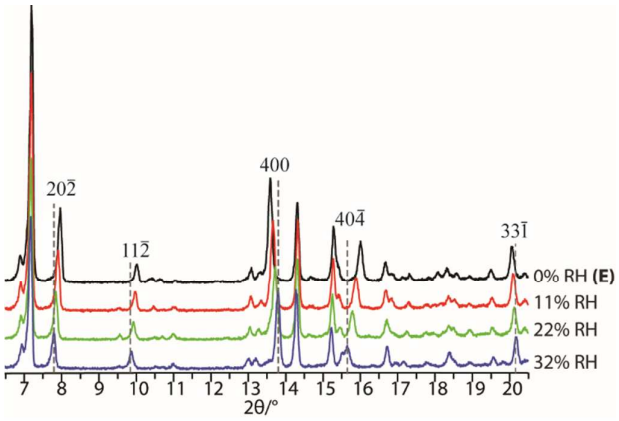

Figure 8. PXRD patterns of the SQ-HCl form NSH under different relative humidity conditions.

3.5. Crystal structures. In this work, the crystal structures of A, B, B', C, D, E, and MH have been determined from PXRD data because numerous attempts to grow single crystals were unsuccessful, with only microcrystalline powders being obtained, while the structure of DH was determined using SCXRD data. Unfortunately, no acceptable structure solution was found for the form DH-II, thus only the unit cell parameters determined after indexing are given. The crystallographic data for all forms is summarized in Table 1. In order to validate the crystal structures of SQ-HCl determined from the PXRD data and obtain the total cell energy, relaxation of the positions of all atoms with fixed unit cell parameters was carried out, using periodic DFT calculations in Quantum ESPRESSO software. The optimized and experimentally determined crystal structures were in good agreement (see Figures S6-S12), Supporting Information) indicating that the determined structures are close to the energy minima within the given space group and unit cell parameters. Crystal structures of forms A, B, B', and DH were solved in the triclinic system with *P*–1 space group and contains one sequifenadine cation and one chloride anion in the asymmetric unit, except for DH, which has additional two water molecules in the asymmetric unit. Forms C, D and E crystallize in the monoclinic system with $P2_1/c$,

$P2_1/n$ and C2/c space groups, respectively, and contain two sequifenadine cations and two chloride anions in the asymmetric unit. Hydrates MH and DH-II crystallize in monoclinic system *C*2/*c* space group with *Z'=1*.

3.5.1. Conformation. The overlay of the all symmetry-independent sequifenadine cations from the crystal structures are shown in Figure 9, and torsion angle values are summarized in Table 4. In sequifenadine cation conformational difference arise mainly due to rotation of methylphenyl groups and quinuclidine moiety around bonds C(1)–C(2), C(1)–C(3), and C(1)–C(5). However, molecular conformations in most of the crystal structures were found to be nearly identical, except for the conformer 1 in form C (designated C1) and for the conformer 2 in form D (D2), colored light blue and red in Figure 9, respectively. Moreover, in conformer D2 the only major conformation difference is that one methylphenyl group is rotated by ~180°, while in the conformer C1 both methylphenyl groups are rotated by 95 – 110°. To determine which of the conformers (C1, D2 or the one observed in all other crystal structures) has lower energy (i.e. is more stable), full *in vacuo* geometry optimization for all the 11 starting geometries was performed. Energy-minimized geometry was highly similar to the starting geometry taken from the crystal structures and identical for all similar conformers (all except for C1 and D2). It was found that the energies of the conformers C1 and D2 are almost identical, while the conformer observed in all other crystal structures is lower in energy by 8.6 $kJ \cdot mol^{-1}$.

Therefore, the observation that the form D (containing less favorable conformer D2) is the most stable polymorph (according to both slurry bridging experiments and full energy calculation in Quantum ESPRESSO) means that intermolecular interactions in this form are significantly energetically more favorable, than those in other polymorphs.

PES scans with respect to flexible torsion angles, performed in Gaussian 09, were complicated by the fact that other torsion angles changed significantly during these scans. Nevertheless, based on the obtained data it was confirmed that conformer observed in most cases is the most stable (designated GM), while confomers D2 and C1 correspond to one of the local energy minima (designated LM1 and LM2).

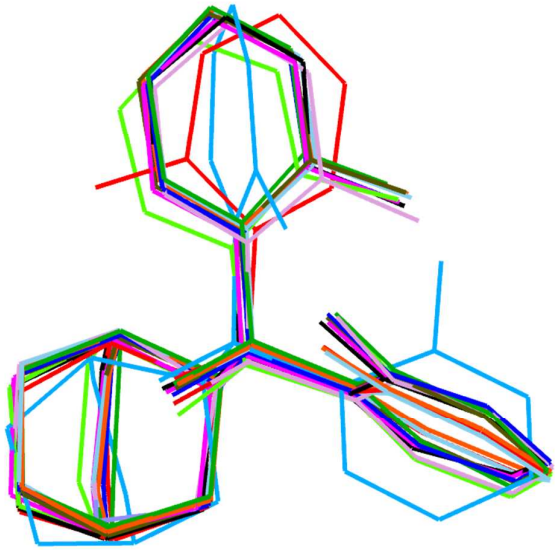

Figure 9. Superimposition of the sequifenadine cation geometries extracted from the crystal structures of A (black), B (green), B' (yellow), C1 (light blue), C2 (violet), D1 (blue), D2 (red), E1 (brown), E2 (orange), MH (lime) and DH (pink).

Table 4. Torsion angles (◦) for conformers in structures of A, B, B', C, D, E, MH, and DH as well as for optimized conformers in local minima (LM1 and LM2) and global minimum (GM)

Conformer	τ_1 (C5–C1–C2–C6)	τ_2 (C5–C1–C3–C12)	τ_3 (C3–C1–C5–C18)
A	108.3	5.1	-175.3
B	113.3	2.4	-170.2
B'	111.5	5.1	-175.2
C2	103.8	-0.5	-167.2

D1	110.9	4.7	-172.5
E1	105.4	6.3	-174.9
E2	106.6	15.0	-174.3
MH	100.6	-7.0	-171.9
DH	105.8	6.4	-171.4
Optimized geometry GM	105.1	8.45	-172.0
C1	-0.4	100.6	-172.5
Optimized geometry LM2	-2.2	104.6	-166.8
D2	-65.7	18.1	-178.6
Optimized geometry LM1	-71.1	15.13	-174.5

3.5.2. Intermolecular interactions. The hydrogen bonding patterns in SQ-HCl forms A, B, B', C, D, E, MH, and DH are shown in Figure 10, while the intermolecular hydrogen bond geometry is summarized in Table S1, Supporting Information. Forms A, B, and B' are characterized by identical intermolecular hydrogen bonding pattern, where two chloride anions interact with two sequifenadine cations through N21–H···Cl25 and O4–H···Cl25 bonds, and forming a tetramer with the graph set $R_4^2(16)$. Formation of the same hydrogen bonding pattern was also observed in the form E, however, as the tetramer was formed by two symmetrically different SQ cations and two different chloride anions, four different hydrogen bonds are present (N21–H···Cl50, O4–H···Cl25, N46–H···Cl25 and O29–H···Cl50). Although in forms A, B, B' and E strong N-H···Cl, and O-H···Cl hydrogen bonds are very similar, there are differences in formation of the weak intermolecular C-H···Cl hydrogen bonds (for details see Table S1, Supporting Information). There are two

weak intermolecular hydrogen bonds in B and B' structures, whereas three in the structure of form A and five in the structure of form E. The main structural difference between polymorphs B and B' is the location of the chloride anion with respect to the SQ cation, resulting different C-H···Cl interaction. In polymorphic form C, however, there is only one strong hydrogen bond between NH^+ group and Cl^- anion in each asymmetric moiety (graph set D), while the other potential hydrogen bond donor (OH group) does not form any conventional hydrogen bonds, however there are 6 weak intermolecular C-H···Cl bonds that compensate for a lack of the O-H···Cl hydrogen bonds. In form D sequifenadine cations and chloride anions do not form tetramers, but instead are connected by one-dimensional infinite chains of hydrogen bonds along the *a*-axis, characterized by graph set $C_4^2(16)$. Each chloride anion is connected to two symmetrically different sequifenadine cations through N21–H···Cl25, O4–H···Cl50, N46–H···Cl50, and O29–H···Cl25 bonds. In form MH there is a similar hydrogen bonding configuration as in forms A, B, B' and E, although, due to the incorporation of water molecules, a hexamer is formed instead. Two sequifenadine cations, two chloride anions and two water molecules form a hexamer with graph set $R_6^4(20)$ through N21–H···Cl25, O4–H···O26, and O26–H···Cl25 interactions. In DH structure, six different conventional hydrogen bonds are present. As in form MH, two sequifenadine cations, two chloride anions and two water molecules form a hexamer with graph set $R_6^4(20)$, but the hydrogen bonds formed are different (O4–H···Cl25, N21–H···O27 and O27–H27A···Cl25). In fact, DH is the only SQ-HCl structure where the N–H···Cl hydrogen bonds are not present. Besides, the Cl^- is the acceptor for two additional hydrogen bonds with water molecules: O26–H26A···Cl25 and O26–H26B···Cl25, forming a hydrogen bonded ring, characterized by graph set $R_4^2(8)$. Additionally, water molecules and chloride anion form one-dimensional

infinite hydrogen bond chains $C_4^2(16)$ along the *a*-axis. It appears that this complex hydrogen bond network in DH structure is very efficient and therefore explains the observed stability of this form.

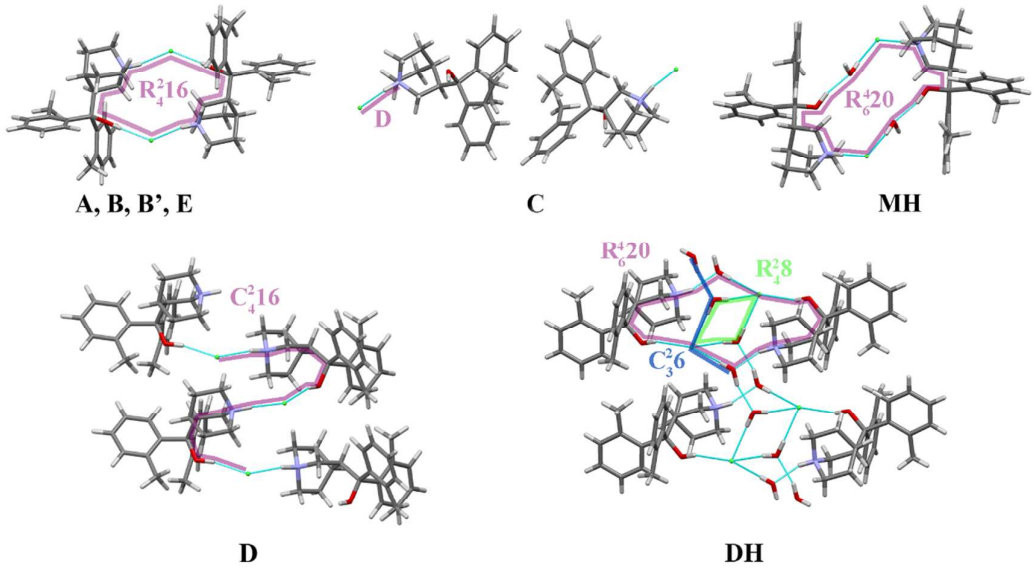

Figure 10. The hydrogen bonding patterns in SQ-HCl forms A, B, B', C, D, E, MH, and DH.

To investigate the energetics of the characteristic intermolecular interactions observed in SQ-HCl polymorphs, interaction energies corresponding to ions interacting via conventional hydrogen bonds were calculated. The obtained data are given in Table S2, Supporting Information. It shows that the most efficient interactions are in the structure of the form D which are 12 – 36 kJ / mole of SQ-HCl more efficient than in other SQ-HCl polymorphs, where sequifenadine cations form two hydrogen bonds. This is probably one of the main reasons leading to D as the most stable polymorph. Nevertheless, in this case it is not possible to distinguish, whether this is due to stronger hydrogen bonds or more efficient electrostatic interactions resulting from different molecular packing. Besides, due to these

electrostatic interactions, different molecular packing can strongly alter the intermolecular interaction energy between other SQ moieties as well.

Evidently, one of the main reasons for low thermodynamic stability of C is the formation of only one hydrogen bond by the sequifenadine cations.

3.5.3. Molecular packing in SQ-HCl polymorphs. Representation of molecular packing in SQ-HCl polymorphs and solvates is given in Figure S13, Supporting Information. The XPac[35] and Mercury software were used to establish the relationship between all crystalline forms with regard to their molecular packing similarities. Based on the characteristic hydrogen bonding motifs three building blocks for all five SQ-HCl polymorphs can be identified: already mentioned $R_4^2(16)$ tetramers, SQ cation and Cl anion pair further forming tetramer $R_4^2(10)$ by additionally employing weak hydrogen bonds (both 0D building blocks), as well as already mentioned $C_4^2(16)$ chains (1D building block), all shown in Figure 11. 3D packing of these building blocks results in formation of structures of polymorphs E, C, and D, while $R_4^2(16)$ tetramers can additionally form 2D layers, by stacking of 1D chains of such tetramers (see Layer 1 in Figure 11). Parallel stacking of such layers above each other results in the structure of polymorph A (stacking mode 1-1-1 in Figure 11), whereas stacking of such layers, so that adjacent layers are shifted by 1 SQ cation, results the structures of B and B' (stacking mode 1-1'-1 in Figure 11). As expected, forms B and B' have very similar crystal packing due to similarity in the 3D arrangement of the ions, with the most important difference being shift in the location of chloride anion. In a more detailed analysis of common building elements in SQ-HCl structures four 0D building blocks were identified: already mentioned $R_4^2(16)$ tetramers and $R_4^2(10)$ tetramers, as well as two SQ cation dimers interacting via dispersion or other weak intermolecular interactions, see Figure S14, Supporting information.

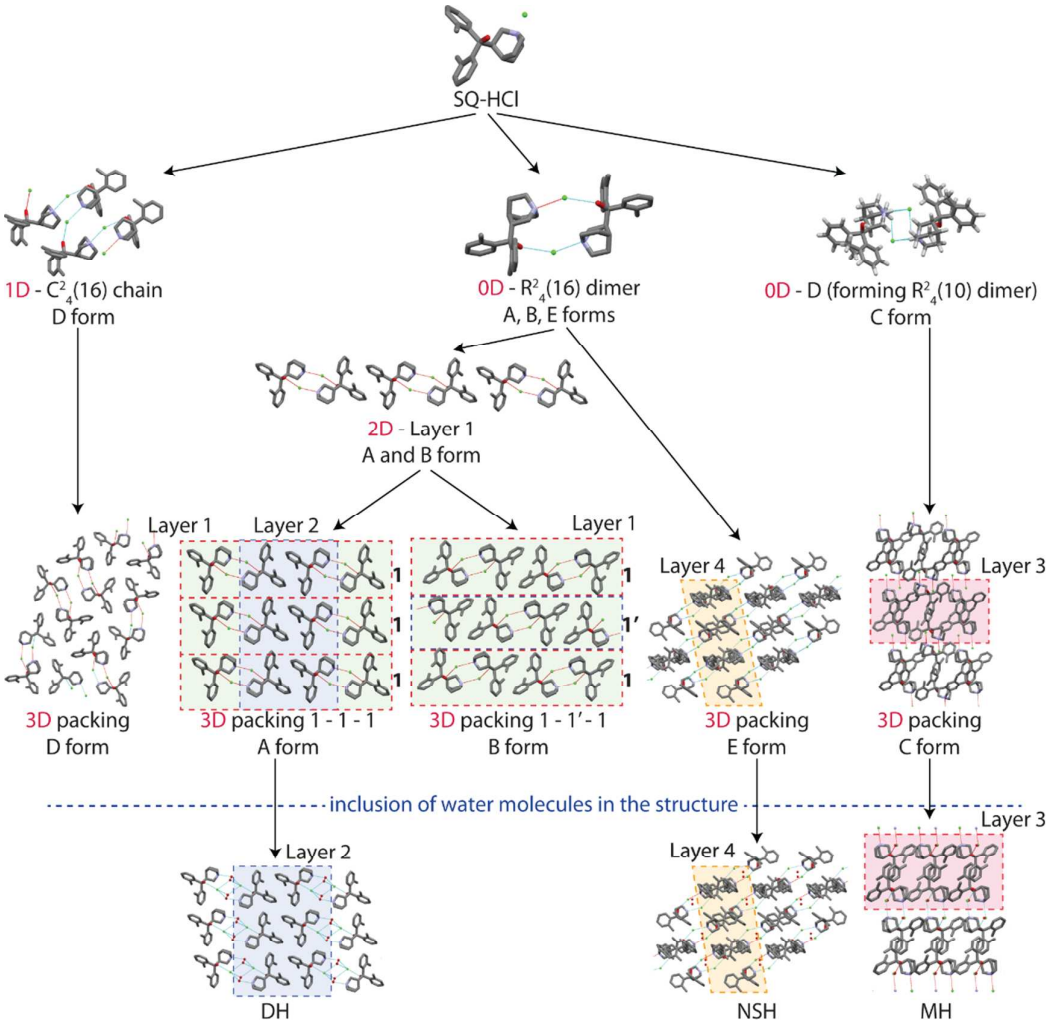

Figure 11. Building and packing similarities in SQ-HCl polymorphs and hydrates (layer 1 is colored green, layer 2 is colored blue, layer 3 is colored red and layer 4 is colored orange).

3.5.4. Incorporation of water molecules in SQ-HCl structures. Comparison of molecular packing in SQ-HCl polymorphs and hydrates reveals that all hydrate structures appear as derived from those of particular polymorphs, by incorporation of water molecules between layers or in structure voids. As can be seen in Figure 11, layer 2 is observed in both structures of A and of DH, while layer 3 is common for

structures of C and MH (although here half of the molecules have different molecular conformation). The water molecules are incorporated between these layers by thus introducing no other significant change in the molecule packing except for the increase of the space between the layers. This packing similarity explains the observation that the dehydration of DH leads to form A and dehydration of MH leads to form C. Therefore, these reversible transformations require only minor molecular reorganization, which explains very easy and reversible transformation between the hydrates (DH and MH) and the respective anhydrous forms (A and C respectively).

As expected, NSH and its isostructural dehydrate E share an identical 3D packing, as water molecules are situated in the voids of structure of polymorph E, see Figure 12. Additionally, layer 4 is common for both structures of E and of NSH, and is the most invariable and characteristic part of these structures. Water molecules in NSH form hydrogen bond with chloride anion while only dispersion interactions are formed with SQ cation.

Typically, the unit cell of nonstoichiometric hydrates expands during sorption and contracts during desorption [36–38], but in this case the volumes of fully dehydrated structure (form E) and NSH structure, containing maximum detected amount of water (at RH=32%), are almost the same (see Table 1). Figure 12 shows that form E contains 8 water accessible voids with the total volume of about 645 $Å^3$(calculated in Mercury with default parameters using contact surface), which is about the same as the volume occupied by the 16 water molecules (2 per asymmetric unit) in the NSH structure with the monohydrate stoichiometry. As the positions of the voids in form E and the positions of the water molecules in NSH are identical, the voids are created due to the loss of the water molecules. Interestingly, after the dehydration structure does not shrink, explaining almost identical volumes of both forms. However, there

are still small voids in NSH structure because only part of the voids in E structure is filled by the water molecules. More detailed analysis, however, showed, that insertion of water molecules increases the distance between layers 4 (increase of lattice parameter *c* by 1.4% and shift of peaks (202) and (404) to higher *d* values, see Figure 8), whereas the packing in other crystallographic directions becomes more compact (decrease of lattice parameters *a* and *b* by 0.5% and 0.3% and shift of peak (400) to lower *d* values, see Figure 8).

Similar incorporation of water molecules in structures of B and D is not possible since there are no structure voids nor layers, between which water molecules could squeeze in with retention of efficient packing. The obtained crystallographic data (see Table 1) and observed phase transformations suggest that the crystal structure of DH-II is similar to that of MH (and therefore also C), with additional water molecules in the crystal structure.

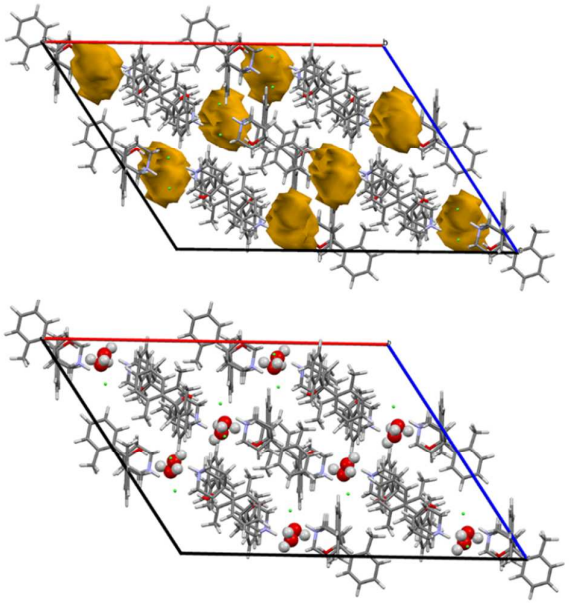

Figure 12. Crystal structure of form E with structure voids highlighted in brown and crystal structure of NSH with water molecules enlarged for clarity.

4. CONCLUSIONS

In the present work, six new anhydrous polymorphs (A, B, B', C, D and E), two dihydrates (DH and DH-II), a monohydrate (MH) and a nonstoichiometric hydrate (NSH) of SQ-HCl are reported. Polymorph A is obtained by dehydration of the dihydrate DH or by recrystallization from tetrahydrofuran. Polymorph B is obtained by recrystallization from acetone, polymorph D is obtained by slurring anhydrous SQ-HCl in *n*-propanol. The methanol and *n*-propanol solvates are used as precursors to obtain C and E polymorphs through the thermal desolvation, whereas polymorph B' is obtained by exposing other SQ-HCl polymorphs (except for the D) to elevated temperature. All of the hydrates are obtained by exposing particular SQ-HCl polymorphs or lower stoichiometry hydrates to particular relative humidity.

Thermodynamic stability of polymorphs has been established from thermal analysis, slurry-bridging experiments and DFT calculations, confirming that stability at ambient temperature follows the order of D>B>A>E>C, while form B' is stable at elevated temperature. DVS and DSC analysis confirms that DH is the most stable hydrate.

Although three different conformations of sequifenadine cation are observed in SQ-HCl polymorph structures, structural analysis showed that the major difference between all polymorphs is the mode of packing of the SQ and chloride ions in the crystal structures, with three different hydrogen bonding patterns being one of the building elements resulting in different molecular packing. All hydrate structures appear as derived from those of particular polymorphs by incorporation of water molecules between layers or in structure voids. The products of phase transformations during the hydration and dehydration confirms the observed structural similarities,

while the ease of these transformations approves the limited structural change involved in this process, as suggested by the structure analysis.

ASSOCIATED CONTENT

Supporting Information. Additional data from the variable temperature PXRD measurements, comparison of experimental and optimized crystal structures, analysis of molecular packing, as well as intermolecular interactions and their energy are presented in the Supporting Information, along with X-ray crystallographic information file (CIF). This information is available free of charge via the internet at http://pubs.acs.org/. Crystallographic information file is also available from the Cambridge Crystallographic Data Center (CCDC) upon request (http://www.ccdc.cam.ac.uk, CCDC deposition number 1510409-1510417).

REFERENCES

(1) Hilfiker, R. In *Crystallization*; Beckmann, W., Ed.; Wiley-VCH Verlag GmbH & Co. KGaA: Weinheim, Germany, 2013; pp 85–103.

(2) Brittain, H. G. *J. Pharm. Sci.* **2012**, *101*, 464–484.

(3) Vangala, V. R.; Chow, P. S.; Tan, R. B. H. *CrystEngComm* **2013**, *15*, 878–889.

(4) Zhang, Q.; Lu, L.; Dai, W.; Mei, X. *CrystEngComm* **2014**, *16*, 1919-1926.

(5) Wang, X.; Wu, S.; Dong, W.; Gong, J. *Org. Process Res. Dev.* **2013**, *17*, 1110–1116.

(6) Zeidan, T. A.; Trotta, J. T.; Chiarella, R. A.; Oliveira, M. A.; Hickey, M. B.; Almarsson, Ö.; Remenar, J. F. *Cryst. Growth Des.* **2013**, *13*, 2036–2046.

(7) Yu, L.; Stephenson, G. A.; Mitchell, C. A.; Bunnell, C. A.; Snorek, S. V; Bowyer, J. J.; Borchardt, T. B.; Stowell, J. G.; Byrn, S. R. *J. Am. Chem. Soc.*

2000, *122*, 585–591.

(8) Pudipeddi, M.; Serajuddin, A. T. M. *J. Pharm. Sci.* **2005**, *94*, 929–939.

(9) Van Tonder, E. C.; Maleka, T. S. P.; Liebenberg, W.; Song, M.; Wurster, D. E.; de Villiers, M. M. *Int. J. Pharm.* **2004**, *269*, 417–432.

(10) Guo, F.; Harris, K. D. M. *J. Am. Chem. Soc.* **2005**, *127*, 7314–7315.

(11) Trask, A. V.; van de Streek, J.; Motherwell, W. D. S.; Jones, W. *Cryst. Growth Des.* **2005**, *5*, 2233–2241.

(12) Zhou, Y.; Guo, F.; Hughes, C. E.; Browne, D. L.; Peskett, T. R.; Harris, K. D. M. *Cryst. Growth Des.* **2015**, *15*, 2901–2907.

(13) Lim, G. K.; Fujii, K.; Harris, K. D. M.; Apperley, D. C. *Cryst. Growth Des.* **2011**, *11*, 5192–5199.

(14) Fujii, K.; Uekusa, H.; Itoda, N.; Yonemochi, E.; Terada, K. *Cryst. Growth Des.* **2012**, *12*, 6165–6172.

(15) Gankina, E. M.; Porodenko, N. V.; Kondratenko, R. Y.; Severin, E. S.; Kaminka, M. E.; Mashkovskii, M. D. *Pharm. Chem. J.* **1992**, *26*, 373–376.

(16) Mashkovsky, M. D.; Yakhontov, L. N. In *Progress in Drug Research / Fortschritte der Arzneimittelforschung / Progrès des recherches pharmaceutiques*; Birkhäuser Basel: Basel, 1969; 13, pp 293–339.

(17) Kons, A.; Rutkovska, L.; Bērziņš, A.; Bobrovs, R.; Actiņš, A. *CrystEngComm* **2015**, *17*, 3627–3635.

(18) Dolomanov, O. V.; Bourhis, L. J.; Gildea, R. J.; Howard, J. A. K.; Puschmann, H. *J. Appl. Crystallogr.* **2009**, *42*, 339–341.

(19) Sheldrick, G. M. *Acta Crystallogr. Sect. A Found. Crystallogr.* **2008**, *64*, 112–122.

(20) Macrae, C. F.; Bruno, I. J.; Chisholm, J. A.; Edgington, P. R.; McCabe, P.; Pidcock, E.; Rodriguez-Monge, L.; Taylor, R.; van de Streek, J.; Wood, P. A. *J. Appl. Crystallogr.* **2008**, *41*, 466–470.

(21) Greenspan, L. *J. Res. Natl. Bur. Stand. Sect. A Phys. Chem.* **1977**, *81A*, 89–96.

(22) Altomare, A.; Cuocci, C.; Giacovazzo, C.; Moliterni, A.; Rizzi, R.; Corriero, N.; Falcicchio, A. *J. Appl. Crystallogr.* **2013**, *46*, 1231–1235.

(23) Altomare, A.; Campi, G.; Cuocci, C.; Eriksson, L.; Giacovazzo, C.; Moliterni, A.; Rizzi, R.; Werner, P.-E. *J. Appl. Crystallogr.* **2009**, *42*, 768–775.

(24) Boultif, A.; Louër, D. *J. Appl. Crystallogr.* **2004**, *37*, 724–731.

(25) Le Bail, A.; Duroy, H.; Fourquet, J. L. *Mater. Res. Bull.* **1988**, *23*, 447–452.

(26) Dollase, W. A. *J. Appl. Crystallogr.* **1986**, *19*, 267–272.

(27) March, A. *Z. Kristallogr.* **1932**, *81*, 285–297.

(28) Giannozzi, P.; Baroni, S.; Bonini, N.; Calandra, M.; Car, R.; Cavazzoni, C.; Ceresoli, D.; Chiarotti, G. L.; Cococcioni, M.; Dabo, I.; Dal Corso, A.; de Gironcoli, S.; Fabris, S.; Fratesi, G.; Gebauer, R.; Gerstmann, U.; Gougoussis, C.; Kokalj, A.; Lazzeri, M.; Martin-Samos, L.; Marzari, N.; Mauri, F.; Mazzarello, R.; Paolini, S.; Pasquarello, A.; Paulatto, L.; Sbraccia, C.; Scandolo, S.; Sclauzero, G.; Seitsonen, A. P.; Smogunov, A.; Umari, P.; Wentzcovitch, R. M. *J. Phys. Condens. Matter* **2009**, *21*, 395502.

(29) Perdew, J. P.; Burke, K.; Ernzerhof, M. *Phys. Rev. Lett.* **1996**, *77*, 3865–3868.

(30) Grimme, S. *J. Comput. Chem.* **2006**, *27*, 1787–1799.

(31) Standard Solid State Pseudopotential Libery (http://www.quantum-espresso.org/pseudopotentials).

(32) Lund, A. M.; Orendt, A. M.; Pagola, G. I.; Ferraro, M. B.; Facelli, J. C. *Cryst. Growth Des.* **2013**, *13*, 2181–2189.

(33) Frisch, M. J.; Trucks, G. W.; Schlegel, H. B.; Scuseria, G. E.; Robb, M. A.; Cheeseman, J. R.; Scalmani, G.; Barone, V.; Mennucci, B.; Petersson, G. A.; Nakatsuji, H.; Caricato, M.; Li, X.; Hratchian, H. P.; Izmaylov, A. F.; Bloino, J.; Zheng, G.; Sonnenberg, J. L.; Hada, M.; Ehara, M.; Toyota, K.; Fukuda, R.; Hasegawa, J.; Ishida, M.; Nakajima, T.; Honda, Y.; Kitao, O.; Nakai, H.; Vreven, T.; Montgomery, J. A. J.; Peralta, J. E.; Ogliaro, F.; Bearpark, M.; Heyd, J. J.; Brothers, E.; Kudin, K. N.; Staroverov, V. N.; Kobayashi, R.; Normand, J.; Raghavachari, K.; Rendell, A.; Burant, J. C.; Iyengar, S. S.; Tomasi, J.; Cossi, M.; Rega, N.; Millam, J. M.; Klene, M.; Knox, J. E.; Cross, J. B.; Bakken, V.; Adamo, C.; Jaramillo, J.; Gomperts, R.; Stratmann, R. E.; Yazyev, O.; Austin, A. J.; Cammi, R.; Pomelli, C.; Ochterski, J. W.; Martin, R. L.; Morokuma, K.; Zakrzewski, V. G.; Voth, G. A.; Salvador, P.; Dannenberg, J. J.; Dapprich, S.; Daniels, A. D.; Farkas, O.; Foresman, J. B.; Ortiz, J. V; Cioslowski, J.; Fox, D. J.; Montgomery, J. A., J.; Peralta, J. E.; Ogliaro, F.; Bearpark, M.; Heyd, J. J.; Brothers, E.; Kudin, K. N.; Staroverov, V. N.; Kobayashi, R.; Normand, J.; Raghavachari, K.; Rendell, A.; Burant, J. C.; Iyengar, S. S.; Tomasi, J.; Cossi, M.; Rega, N.; Millam, N. J.; Klene, M.; Knox, J. E.; Cross, J. B.; Bakken, V.; Adamo, C.; Jaramillo, J.; Gomperts, R.; Stratmann, R. E.; Yazyev, O.; Austin, A. J.; Cammi, R.; Pomelli, C.; Ochterski, J. W.; Martin, R. L.; Morokuma, K.; Zakrzewski, V. G.; Voth, G. A.; Salvador,

P.; Dannenberg, J. J.; Dapprich, S.; Daniels, A. D.; Farkas, Ö.; Foresman, J. B.; Ortiz, J. V; Cioslowski, J.; Fox, D. J. *Gaussian 09, Revision D.01*; Gaussian Inc., Wallingford, CT, 2009.

(34) Burger, A.; Ramberger, R. *Mikrochim. Acta* **1979**, *72*, 259–271.

(35) Gelbrich, T.; Hursthouse, M. B. *CrystEngComm* **2005**, *7*, 324–336.

(36) Pina, M. F.; Pinto, J. F.; Sousa, J. J.; Fábián, L.; Zhao, M.; Craig, D. Q. M. *Mol. Pharm.* **2012**, *9*, 3515–3525.

(37) Fujii, K.; Aoki, M.; Uekusa, H. *Cryst. Growth Des.* **2013**, *13*, 2060–2066.

(38) Kiang, Y.-H.; Cheung, E.; Stephens, P. W.; Nagapudi, K. *J. Pharm. Sci.* **2014**, *103*, 2809–2818.

FOR TABLE OF CONTENTS USE ONLY

POLYMORPHS AND HYDRATES OF SEQUIFENADINE HYDROCHLORIDE: CRYSTALLOGRAPHIC EXPLANATION OF OBSERVED PHASE TRANSITIONS AND THERMODYNAMIC STABILITY

Artis Kons, Agris Bērziņš and Andris Actiņš

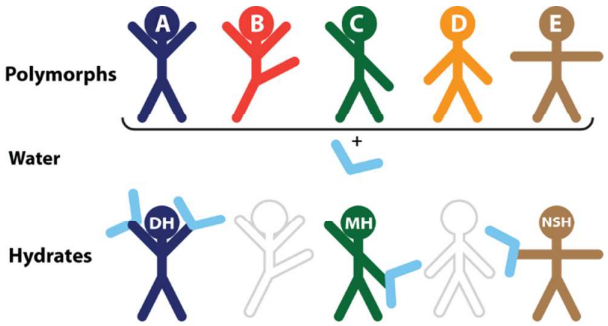

In this study, detailed analysis of crystal structures was used to rationalize the observed stability and phase transformations of sequifenadine hydrochloride polymorphs and hydrates, as well as to understand the observed structural diversity.